8

NASA CR- 114293
AVAILABLE TO THE PUBLIC

PAET AFTERBODY THERMAL PERFORMANCE AND COMPONENT STRUCTURAL PROPERTIES

by David L. Carlson

April, 1971

Prepared under Contract No. NAS2-6274 by

MARTIN MARIETTA CORPORATION
Denver, Colorado

for

AMES RESEARCH CENTER
NATIONAL AERONAUTICS AND SPACE ADMINISTRATION

NASA CR-114293

PAET AFTERBODY THERMAL PERFORMANCE AND COMPONENT MECHANICAL PROPERTIES

by David L. Carlson

April, 1971

Approved by: [signature]
D. V. Sallis
Program Manager

Prepared under Contract No. NAS2-6274 by

MARTIN MARIETTA CORPORATION
Denver, Colorado

for

AMES RESEARCH CENTER
NATIONAL AERONAUTICS AND SPACE ADMINISTRATION

ABSTRACT

This report summarizes the results of three tasks conducted by the Martin Marietta Corporation for NASA/AMES Research Center under contract NAS2-6274. This study was conducted during the period of December 7, 1970 through March 26, 1971. The specific tasks were:

Task I, the calculation of the thermal response of the PAET afterbody ablator /structure and of the afterbody/forebody interface region;

Task II, the fabrication and test of SLA-220-ablator/PAET structure plasma arc specimens; and

Task III, the experimental determination of the PAET afterbody component structural properties.

TABLE OF CONTENTS

		Page
ABSTRACT		i
TABLE OF CONTENTS		ii
LIST OF TABLES		iii
LIST OF FIGURES		iv
I.	INTRODUCTION AND SUMMARY	1
II.	PAET AFTERBODY HEAT SHIELD THERMAL ANALYSIS	2
	A. REFERENCE CONVECTIVE HEAT TRANSFER DATA	2
	B. THERMOPHYSICAL PROPERTIES	3
	C. ONE-DIMENSIONAL THERMAL ANALYSES	4
	D. THREE-DIMENSIONAL THERMAL ANALYSES	5
III.	FABRICATION AND TEST OF SLA-220 PLASMA ARC SPECIMENS	8
	A. THREE-INCH DIAMETER SPECIMENS	8
	B. ELEVEN-INCH DIAMETER SPECIMENS	9
IV.	PAET AFTERBODY COMPONENT STRUCTURAL PROPERTIES	10
	A. PAET-HONEYCOMB-SANDWICH THERMAL EXPANSION	10
	B. PAET-HONEYCOMB-SANDWICH FLEXURE STRENGTH	10
	C. PAET-FACE-SHEET-TO-CORE TENSILE AND FACE-SHEET-TO-ALUMINUM SHEAR STRENGTH	11
	D. SLA-220/PAET-HONEYCOMB-SANDWICH BOND STRENGTH	12
V.	CONCLUSIONS	12
VI.	REFERENCES	15
VII.	TABLES	17-22
VIII.	FIGURES	23-51

PRECEDING PAGE BLANK NOT FILMED

LIST OF TABLES

TABLE I	PAET Hypersonic Reentry Trajectory and Reference Heating Environment
TABLE II	PAET Subsonic Reference Heating Environment
TABLE III	Aluminum Thermophysical Properties
TABLE IV	High Silica Glass-Phenolic Thermophysical Properties
TABLE V	Honeycomb core Thermophysical Properties
TABLE VI	Glass-Epoxy Thermophysical Properties
TABLE VII	Final-Attachment-Line-Gasket Thermophysical Properties
TABLE VIII	Values of $\dot{q}/\dot{q}_s$ for Three Dimensional Windward Corner Analyses, from Reference 7
TABLE IX	Summary of Surface Recession Predictions and Virgin Ablator Thicknesses Remaining, Three-Dimensional Windward Corner Analyses
TABLE X	Plasma Arc Specimen Thermocouple Locations

LIST OF FIGURES

FIGURE 1. PAET Probe

FIGURE 2. Variable $\dot{q}/\dot{q}_s$ for One-Dimensional Thermal Analysis

FIGURE 3. Model for One-Dimensional PAET Afterbody Thermal Analysis

FIGURE 4. PAET Afterbody Thermal Response, $\dot{q}/\dot{q}_s = 0.05$, One-Dimensional Analysis

FIGURE 5. PAET Afterbody Thermal Response, $\dot{q}/\dot{q}_s = 0.10$, One-Dimensional Analysis

FIGURE 6. PAET Afterbody Thermal Response, Variable $\dot{q}/\dot{q}_s$, One-Dimensional Analysis

FIGURE 7. Model for Three-Dimensional Analysis of PAET Windward Corner

FIGURE 8. PAET Surface Temperature Response, Nominal Heating Distribution, Three-Dimensional Windward Corner Analysis

FIGURE 9. PAET Surface Temperature Response, 1.5 x Nominal Heating Distribution, Three-Dimensional Windward Corner Analysis

FIGURE 10. PAET Structure Temperature Response, Nominal Heating Distribution, Three Dimensional Windward Corner Analysis

FIGURE 11. PAET Structure Temperature Response, 1.5 x Nominal Heating Distribution, Three-Dimensional Windward Corner Analysis

FIGURE 12. Comparison of One-Dimensional and Three-Dimensional PAET Afterbody Thermal Response, Nominal Heating Distribution

FIGURE 13. Plasma Arc Specimen 2-2-1 Thermal Response

FIGURE 14. Plasma Arc Specimen 2-2-2 Thermal Response

FIGURE 15. Plasma Arc Specimen 2-2-3 Thermal Response

FIGURE 16. Plasma Arc Specimen 2-2-1 After Test

FIGURE 17. Plasma Arc Specimen 2-2-2 After Test

FIGURE 18. Plasma Arc Specimen 2-2-3 After Test

LIST OF FIGURES (continued)

FIGURE 19. PAET RF Transmission Test Panels After Test

FIGURE 20. PAET-Honeycomb-Sandwich Thermal Expansion Data

FIGURE 21. PAET-Honeycomb-Sandwich Flexure Strength and Modulus Parallel to Core Ribbon

FIGURE 22. PAET-Honeycomb-Sandwich Flexure Strength and Modulus, Perpendicular to Core Ribbon

FIGURE 23. Typical PAET-Honeycomb-Sandwich Flexure Specimen After Test

FIGURE 24. Typical PAET-Honeycomb-Sandwich Flexure Specimen After Test

FIGURE 25. PAET-Honeycomb-Sandwich Face-Sheet-To-Core Tensile and Face-Sheet-To-Aluminum Shear Strength

FIGURE 26. Typical Face-Sheet-To-Core Tensile Specimen

FIGURE 27. Typical Face-Sheet-To-Aluminum Lap Shear Specimen

FIGURE 28. SLA-220/PAET-Honeycomb-Sandwich-Face-Sheet Bond Ultimate Tensile Strength

FIGURE 29. Typical SLA-220-To-Face-Sheet Tensile Specimen

I. INTRODUCTION AND SUMMARY

The Planetary Atmospheric Experiments Test (PAET) ablative afterbody heat shield was designed* to meet requirements specified by NASA/AMES Research Center. The heat shield is basically two separate systems, the forebody ablative heat shield consisting of 0.30" of PAET 28, a low density filled silicone, bonded to the conical aluminum forebody structural shell. The afterbody ablative heat shield consists of 0.25" of SLA-220, also a low density filled silicone, bonded to the hemispheric afterbody structure. The afterbody structure is a ½" thick honeycomb sandwich consisting of single glass-epoxy face sheets over flexible glass-phenolic honeycomb. A sketch of the PAET reentry body is presented in Figure 1. Both the forebody and afterbody structures were manufactured by NASA/AMES Research Center, while the ablative heat shields were fabricated on the structures by Martin Marietta Corporation.

The design heating environment for the afterbody heat shield was 5% of the stagnation heating rate. The thermal analyses reported herein were undertaken to evaluate the thermal response of the PAET afterbody ablative heat shield to off-design conditions. One-dimensional thermal analyses were performed at three levels of heating, along with three-dimensional analyses of the windward corner of the PAET reentry body at two levels of heating.

In Task II, a total of thirteen plasma arc specimens were fabricated, ten of which were delivered to NASA/AMES Research Center on March 12, 1971. The remaining three were tested by Martin Marietta Corporation to determine the experimental thermal response of the SLA-220-ablative/structure system.

* See Reference 1 for details of the design and fabrication of the PAET Ablative Heat Shields.

The structural properties of the PAET-afterbody-honeycomb-sandwich and the ultimate tensile strength of the bond of SLA-220-to-honeycomb-face-sheet were determined over the temperature range from room temperature up to 375°F. The thermal expansion of the PAET-honeycomb-sandwich material was also determined, at temperatures up to 450°F.

II. PAET AFTERBODY HEAT SHIELD THERMAL ANALYSIS

A. Reference Convective Heating Data

The aerodynamic heating environment and heating distributions during the hypersonic reentry were supplied by NASA/AMES Research Center. The reentry trajectory and stagnation point heating rate was specified to be the same as used in Contract NAS2-5538, "Heat Shields for Planetary Atmospheric Test Probe."* Table I presents the reentry trajectory data and stagnation point reference heating environment of Contract NAS2-5538.

In the original design, during the subsonic portion of the reentry, the convective heat transfer at the surface of the probe was neglected. Conservatively, only radiation from the ablative surface was considered in the analysis. In the analyses reported herein, convective cooling was included with radiation as a surface boundary condition during the subsonic portion of the reentry. For calculation of the convective heat transfer coefficient, data on the velocity and the free stream density as a function of time were obtained from Reference 2, and are documented in Table II.

The heat transfer coefficient was calculated using an empirical expression** for the average heat transfer

* See Reference 1
** See References 3 and 4

coefficient to a spherical body. As an approximation, the local convective heat transfer coefficient to the PAET ablative heat shield was assumed equal to the average heat transfer coefficient to a sphere of the same diameter. The basis for this assumption is that A) the PAET shape is close to spherical, B) the heat transfer to the separated region on a sphere in subsonic flow is on the order of the stagnation point heat transfer, due to the turbulence in the wake, and C) the heat transfer to a point on a sphere 90° from the stagnation point is close to the average heat transfer coefficient due to the large area of this region relative to the stagnation region.

The velocity, free stream density, and heat transfer coefficient calculations are presented in Table II.

B. Thermophysical Properties

For this task, seven different materials were incorporated in the one-dimensional and/or three-dimensional analyses. The thermophysical properties of the PAET 28 Ablative have been previously presented in Reference 1. The thermophysical properties of the SLA-220 Ablative used in this analyses were the latest set of correlated properties, reported in Reference 5, and previously sent to NASA/AMES Research Center as part of Reference 6.

The thermophysical properties of the five other materials are presented in Tables III through VII.

C. One-Dimensional Thermal Analyses

One-dimensional calculations of the PAET afterbody ablator/structure thermal response were performed for the following three cases of local heat transfer versus time:

1) $\dot{q}/\dot{q}_s$ = 0.05 at supersonic speeds
   = 1.0 at subsonic speeds
2) $\dot{q}/\dot{q}_s$ = 0.10 at supersonic speeds
   = 1.0 at subsonic speeds
3) $\dot{q}/\dot{q}_s$ = function of time shown in Figure 2 at supersonic speeds
   = 1.0 at subsonic speeds

Where $\dot{q}_s$ is the Reference Heating Environment tabulated in Tables I and II.

The model used for the one-dimensional thermal analyses is shown in Figure 3. As noted in the Figure, both radiation between the face sheets and conduction through the honeycomb was considered. In addition, radiation from the inner surface of the afterbody-honeycomb-sandwich-structure to the upper face sheet of the honeycomb-sandwich-Ground-Plane was included.

Temperature as a function of time at selected locations for each heating case are presented in Figure 4 through 6. All three heating cases give consistent results. Note that both the $\dot{q}/\dot{q}_s$ = 0.10, and the variable $\dot{q}/\dot{q}_s$ cases exceed 300°F at the external face sheet, which is the design temperature limit for the PAET afterbody ablator/structure interface. The peak temperatures are 328°F and 307°F respectively. The $\dot{q}/\dot{q}_s$ = 0.05 case reached a maximum temperature at the ablator/structure interface of about 261°F.

A point which may be of more importance is the temperature differential between the external and internal face sheets of the afterbody-honeycomb-sandwich-structures. This differential is a maximum at about 40 seconds in all three cases, with values ranging from about 140°F for the $\dot{q}/\dot{q}_s$ = 0.05 case, about 170°F for the variable $\dot{q}/\dot{q}_s$ case, to about 190°F for the $\dot{q}/\dot{q}_s$ = 0.10 case. This temperature differential may cause significant thermal stresses during reentry.

D. Three-Dimensional Thermal Analyses

Three-dimensional thermal analyses were conducted on the PAET forebody/afterbody interface region, at the windward corner. Two cases of heating environment were used, 1) the experimental heating distributions of Reference 7, and 2) the same heating distributions with a 1.5 factor applied to the heating rate. In both of these cases during subsonic flight the local convective heat transfer rate was set equal to the Reference Heating Environment of Table II.

A sketch of the PAET forebody/afterbody interface region is presented in Figure 7. A large area of the forebody heat shield and structure was included in this analysis due to the large thermal mass and high thermal conductivity of the aluminum forebody structure. The inner surface of the aluminum-forebody-structure was assumed adiabatic due to the low surface emittance of aluminum. The model of the afterbody-honeycomb-sandwich-structure was equivalent to the one-dimensional model, i.e., radiation and conduction between the face sheets were included. The experimental heating rate ratios, from Reference 7, at various locations in the forebody/afterbody interface region are tabulated in Table VIII.

The method of three-dimensional thermal analysis including ablation is based upon the fact that the heat transfer within the ablative materials is essentially one dimensional, due to the relatively small variation in convective heat transfer along the surface. Thus, one is able to set up a series of one-dimensional ablation cases coupled with a three-dimensional conduction/radiation model of the substructure and areas of the ablative materials which do not ablate. Martin Marietta Corporation has a computer program which couples one-dimensional ablation blocks to three-dimensional conduction/radiation elements. However, for the present analyses, since only two heating cases were being analyzed and the geometry is fairly simple, a manual iterative technique was used. One-dimensional ablation cases were run for the various locations on the windward corner, using estimated substructure versus time response as the backface boundary condition. The calculated temperature versus time at respective points in the virgin ablative materials were then input as boundary conditions in the three-dimensional conduction/radiation model.

In both heating cases considered, the second itera on yielded temperatures within a few degrees of the first iteration, and the problems were satisfactorily converged.

The material response predicted by these analyses are summarized in Figures 8 through 11, and Table IX. Figures 8 and 9 are plots of the surface temperature as a function of time at four locations near the forebody/afterbody interface region, for the two cases of heating environment.

Figures 10 and 11 present the corresponding structure temperatures for the two heating cases. The respective surface recession values and the thickness of virgin ablative remaining after reentry are tabulated in Table IX. As one would expect based upon the data of Reference 1, the forebody heat shield system is quite conservatively designed from a thermal standpoint, with peak structure temperatures on the order of 168°F. On the other hand, the predicted thermal response for the afterbody system at the nominal heating environment is quite close to the design temperature limit of 300°F. In the case of the 1.5 factored heating, the afterbody ablator/honeycomb sandwich interface exceeds the design limit, reaching 330°F.

The fast thermal response of the locations F and G relative to locations I, J, and K in Figures 10 and 11 is not unexpected, and is a result of the low thermal mass of the afterbody honeycomb sandwich. The point I, on the afterbody aluminum support ring, follows primarily the forebody aluminum structure response due to the forebody structures' large thermal mass and high thermal conductivity. Although the afterbody honeycomb sandwich does not exceed the design temperature limit in the nominal heating case, large temperature differentials exist between the external face sheet and the internal face sheet (on the order of 185°F for the nominal heating case), as predicted in the one-dimensional analyses. Even more severe is the temperature differential between the external face sheet and the afterbody aluminum support ring, with maximum differential on the order of 190°F for the nominal heating case, and about 220°F for the factored heating case, both occuring at about 50 seconds in time.

The afterbody-heat-shield/honeycomb-sandwich-structure thermal response is essentially independent of the forebody-heat-shield/aluminum-structure/afterbody-aluminum-support-ring thermal response. The lower temperature of the afterbody aluminum support ring does not significantly reduce the temperatures in the honeycomb sandwich structure because of the low thermal conductivity of the glass-epoxy face sheets and SLA-220. This is shown by the comparison in Figure 12, between the three-dimensional thermal response and a one-dimensional analysis at about 1 inch from the afterbody aluminum support ring. Identical local heating environments were used, and the temperatures differ by less than 10°F.

III. FABRICATION AND TEST OF SLA-220 PLASMA ARC SPECIMENS

A. Three-Inch Diameter Specimens

Ten (10) flat-faced "splash type" ablative plasma arc specimens were fabricated with .25 inch of SLA-220 over the PAET-honeycomb-sandwich material. Each specimen was 3.0 inches in diameter, and was instrumented with three 36 gage Chromel-Alumel Thermocouples. Table X tabulates the distance from the surface of the SLA-220 ablative to the respective thermocouples, as measured on X-ray prints of each specimen. The thermocouples were installed in the honeycomb sandwich disk prior to the application of the SLA-220. These ten specimens were shipped to NASA/AMES Research Center on March 12, 1971.

B. Eleven-Inch Diameter Specimens

Three (3) flat-faced "splash type" ablative plasma arc specimens, each eleven inches in diameter, were fabricated with .25 inch of SLA-220 over the PAET-honeycomb-sandwich material. Each specimen was instrumented with three 36 gage Chromel-Alumel Thermocouples. The location of each thermocouple junction as measured on X-ray negatives of each specimen are presented in Table X.

These specimens were tested in the Martin Marietta Corporation Plasma Arc Facility. The following table summarizes the Plasma Arc test conditions to which each specimen was exposed:

Specimen No.	Heating Rate Btu/Ft^2-Sec	Stream Enthalpy Btu/lb	Stagnation Pressure Atmos.	Test Time Sec	Total Heat Btu/Ft^2
2-2-1	7.76	2124	.008	22	176
2-2-2	15.9	4407	.012	10	159
2-2-3	15.9	4385	.012	15	239

The heat pulses for specimens 2-2-1 and 2-2-2 yielded approximately the total heat (160 Btu/Ft^2) predicted for the PAET afterbody, based upon the variable $\dot{q}/\dot{q}_s$ shown in Figure 2 and the reference stagnation heating data of Table I. Specimen 2-2-3 was exposed to a longer heating period to simulate the response to a 50 percent greater total heat input. The measured thermal response for the specimens is presented in Figures 13, 14, and 15 respectively. Note that the ablator initial temperatures are higher than room temperature, up to 240°F. The large size of the specimen prevented full retraction of the specimen out of the test chamber. The result was a small amount of plasma jet plume impingment on the specimens during calibration, prior to test.

Correlation analyses were conducted on each of these tests, with the results shown in Figures 13, 14, and 15. The high degree of agreement between the analysis and the test data verifies our mathematical model of SLA-220 ablative and our predictions of temperatures during reentry.

Despite the high temperatures to which the SLA-220 ablator/structure bond line was exposed (up to 480°F on specimen 2-2-3), the integrity of the ablative material and the bond line were unaffected, with no signs of delamination. There were some cracks in the char normal to the heated surface, as normally occurs in SLA-220. Note the dark surface of the specimens after test (Figures 16, 17, and 18), and compare with the light appearance of specimens tested in radiant heating (see Figure 19), indicating a difference in surface composition. A difference in surface composition may affect the RF transmission characteristics.

IV. PAET AFTERBODY COMPONENT STRUCTURAL PROPERTIES

A. PAET-Honeycomb-Sandwich Thermal Expansion

The thermal expansion of two strips of PAET-honeycomb-sandwich-material was determined over the range of temperatures from room temperature to 450°F. The specimens were two inches wide by eight inches long, one being cut with the honeycomb core ribbon parallel, and the other perpendicular to the eight inch dimension. The test data is presented in Figure 20. Note the large residual strain in the specimen after cool down to room temperature.

B. PAET-Honeycomb-Sandwich Flexure Strength

The ultimate flexure strength of the PAET-honeycomb-sandwich material was measured by testing three-inch by eight-inch flat panels under single point loading with two point simple support. The results of these tests are shown in Figures 21 and 22. These present respectively the data for specimens with the honeycomb ribbon parallel and perpendicular to the specimens' eight-inch dimension. Three specimens were tested at each test point. There is remarkable aggreement between the two sets of data, indicating that the ultimate flexure strength is independent of honeycomb core orientation.

All specimens failed by buckling in the compression face sheet. The post-test appearance of typical specimens is shown in Figure 23. In some cases, local delamination of the compression face sheet occured in the region of the buckling, as shown in Figure 24. However, the delamination never extended more than one core cell width beyond the point of buckling initiation. Note in Figures 21 and 22 a significant reduction in strength at 300°F and above. In order to calculate the strength and modulus data, the face sheet thickness on a number of specimens was measured, yielding an average face sheet thickness of 0.015 inch.

C. PAET Face-Sheet-To-Core Tensile and Face-Sheet-To-Aluminum Shear Strength

The face-sheet-to-core ultimate tensile strength was measured by bonding aluminum pull blocks to two-inch by two-inch squares of PAET-honeycomb-sandwich. Three specimens were tested at each data point, and the test results are presented in Figure 25. Note that there is a significant reduction in tensile strength at temperatures above 300°F. A photograph of typical specimens before and after test is presented in Figure 26.

The double lap shear specimens, which had been fabricated by NASA/AMES Research Center, were modified slightly prior to test in order to prevent tensile failures in the face sheets. The specimens, which were 1.5 inches wide with 1.5 inch overlap, had one side cut at approximately 1/4 inch from the butt joint of the aluminum pull block. Figure 27 shows a typical lap shear specimen after test. Three specimens were tested at each test condition, and the data is presented in Figure 25. There was some evidence that the aluminum shear blocks were not completely cleaned prior to bonding the face sheets on, since mill dye marks were visible through the transparent face sheet material. It is believed that this may have been the cause of the large scatter in the lap shear test data at the lower temperatures.

D. <u>SLA-220/PAET-Honeycomb-Sandwich Bond Strength</u>

The ultimate tensile strength of the bond between the SLA-220 ablative and the PAET-honeycomb-sandwich material was determined on two-inch by two-inch square specimens. The test results are shown in Figure 28. In every case, the failure at ultimate strength was a cohesive failure within the SLA-220 ablative. Typical specimens before and after test are shown in Figure 29.

V. CONCLUSIONS

A. <u>On the Thermal Analyses</u>

1) For the one-dimensional analyses, only the $\dot{q}/\dot{q}_s$ = 0.05 case did not exceed the ablator/honeycomb sandwich interface design temperature limit of 300°F (a peak of 261°F was reached).

2) The cases $\dot{q}/\dot{q}_s$ = 0.10 and $\dot{q}/\dot{q}_s$ = variable reached 328°F and 307°F respectively.

3) The maximum temperature differentials between the afterbody honeycomb sandwich external and internal face sheets are predicted by one-dimensional analyses to be about 140°F for the $\dot{q}/\dot{q}_s$ = 0.05 case, about 190°F for the $\dot{q}/\dot{q}_s$ = variable case. Temperature differentials of

this magnitude during reentry may cause significant thermal stresses.

4) Based upon the three-dimensional thermal analyses, the PAET forebody heat shield is designed quite conservatively, with peak structural temperatures on the order of 168°F.

5) The thermal response of the aluminum afterbody support ring is primarily a function of the forebody aluminum structure thermal response.

6) The thermal response of the afterbody-ablator/honeycomb-sandwich-structure is essentially independent of the forebody-heat-shield/aluminum-structure/aluminum-afterbody-support-ring system.

7) As predicted in the one-dimensional analyses, the three-dimension thermal analyses predict that significant temperature differentials will exist between the afterbody honeycomb sandwich face sheets (about 185°F differential for the nominal heating case), and between the honeycomb structure and the aluminum afterbody support ring. This may result in critical thermal stresses in the glass-epoxy face sheets near the aluminum support ring and in the bond between the face sheets and support ring.

B. <u>On The Plasma Arc Tests</u>

1) The PAET afterbody heat shield will tolerate a significant heating overshoot above design conditions and retain self integrity and integrity in the bond to the honeycomb sandwich.

2) The ablation model for SLA-220 correlates well with test, which verifies the thermal predictions for the reentry.

3) The surface of SLA-220 is darker when tested in a plasma arc as compared with radiant heating tests. This may indicate a difference in RF transmission characteristics due to a difference in surface composition.

C. On the Structural Property Tests

1) The PAET-honeycomb-sandwich material fails in flexure by buckling of the compression face sheet.

2) The SLA-220/PAET-honeycomb-sandwich bond is at least as strong as the cohesive strength of the SLA 220 ablative.

3) While there is a significant reduction in the strength of the PAET-honeycomb-sandwich material at about 300°F, no real conclusions can be drawn from this data until a thorough structural analysis can be accomplished on the PAET heat shield/structure system.

VI. REFERENCES

1) "Heat Shields for Planetary Atmospheric Experiments Test (PAET) Probe, Final Report," MCR-70-170, David L. Carlson, Martin Marietta Corporation, May 20, 1970.

2) Telephone communication with N. S. Vojvodich, December 11, 1970.

3) McAdams, W. H., Heat Transmission, Third Edition, McGraw-Hill Book Company, Inc., 1954.

4) Kreith, Frank, Principles of Heat Transfer, Second Edition, International Textbook Company, 1965.

5) "Correlation of SLA 220 Ablation Properties", SR-1631-69-09, David L. Carlson, Martin Marietta Corporation, September, 1969.

6) Martin Marietta Corporation letter from Dan Sallis to N. S. Vojvodich, NASA/AMES Research Center, Dated November 26, 1969.

7) NASA/AMES Research Center letter from N. S. Vojvodich to Dan Sallis, Martin Marietta Corporation, dated December 4, 1970.

8) Carlson, D. L., and Strauss, E. L. "Signal Transmission Through an RF-Transparent Ablator During Low Heat Flux Exposure", Proceedings of The Tenth Electromagnetic Window Symposium, Georgia Institute of Technology, July 29-31, 1970.

VII TABLES

TABLE I. PAET Hypersonic Reentry Trajectory and Reference Heating Environment

ENTRY CONDITIONS:

ENTRY SPEED=25,000 FT/SEC
M/CDA=.28 SLUGS/FT12
RADIUS=18 INCHES
ENTRY ANGLE = - 30 DEGREES
CONE HALF ANGLE=55 DEGREES

TIME SEC	ALTITUDE FEET	VELOCITY KM/SEC	ENTHALPY cal/gm	CONVECTIVE HEATING RATE cal/gm^2/sec	PRESSURE Atm
0	325000	7.62	6929.12	3.34	.000322
1	313736	7.62	6929.12	4.21	.000594
2	303021	7.63	6947.31	5.38	.0011
3	292608	7.63	6947.31	6.97	.00203
4	281665	7.63	6947.31	9.13	.00375
5	270724	7.63	6947.31	12.1	.00693
6	259426	7.63	6947.31	16	.0128
7	246321	7.61	6910.94	21.2	.0235
8	232160	7.57	6838.48	28.	.0429
9	218023	7.51	6730.51	35.8	.0742
10	206391	7.4	6534.78	42.3	.112
11	194834	7.25	6272.55	48.6	.164
12	183534	7.01	5864.13	53.7	.234
13	172405	6.69	5340.97	56.1	.318
14	162350	6.26	4676.45	54.6	.408
15	153241	5.73	3918.11	48.8	.486
16	145622	5.12	3128.3	39.7	.536
17	138038	4.47	2384.42	30.	.569
18	130811	3.8	1723.2	20.5	.569
19	124854	3.16	1191.63	12.7	.523
20	120000	2.6	806.705	7.24	.454
21	116050	2.14	546.507	3.88	.382
22	112812	1.77	373.865	1.93	.315
23	110133	1.48	261.391	.832	.267

TABLE II. PAET Subsonic Reference Heating Environment

TIME* SEC	V_∞ FT/SEC	ρ_∞ lbm/FT^3	$\left(\frac{V_\infty \rho_\infty D_o}{\mu_f}\right)$** Dimensionless	$\bar{h}$ *** lb/FT^2-SEC
34.5	802	.00319	6.97×10^5	.0055
54.5	503	.00554	7.55×10^5	.00575
74.5	418	.00873	9.95×10^5	.00679
94.5	393	.0126	13.5×10^5	.00815
144.5	239	.0248	16.2×10^5	.00908
194.5	195	.0372	19.8×10^5	.0103
244.5	167	.0505	23.0×10^5	.0112
283.2	151	.0614	25.3×10^5	.0119

* Time from 325000 FT

** μ_f = viscosity of air = 1.1×10^{-5} $\frac{\text{lbm}}{\text{FT-SEC}}$ Do = Probe Diameter = 3 FT

***
References 3 & 4; $\frac{\bar{h}\, D_o C_p}{k_f} = 0.37\left(\frac{V_\infty \rho_\infty D_o}{\mu_f}\right)^{0.6}$

C_p = Specific heat of air = .24 BTU/lb$^\circ$F

k_f = conductivity of air = $.333 \times 10^{-5}$ $\frac{\text{BTU}}{\text{FT-SEC}^\circ\text{F}}$

TABLE III Aluminum Thermophysical Properties

DENSITY: 0.101 lb/in^3

CONDUCTIVITY BTU/IN-SEC°R	SPECIFIC HEAT BTU/lb - °R
.0023	.22

TABLE IV High Silica Glass-Phenolic Thermophysical Properties

DENSITY: 0.0637 lb/in^3

Temperature °R	Conductivity BTU/IN-SEC°R	Specific Heat BTU/lb - °R	Emittance
460	.0000048	.200	.85
660	.0000051	.228	.8
760	.0000052	.238	.85
960	.0000052	.258	.85
1360	.0000052	.275	.85
1560	.0000052	.280	.85
1660	.0000052	.286	.85
1960	.0000052	.343	.85
2160	.0000052	.370	.85

TABLE V Honeycomb Core Thermophysical Properties

BULK DENSITY: 0.00162 lb/in^3

Temperature °R	Effective Conductivity BTU/IN-SEC°R	Specific Heat BTU/lb - °R
360	.00000011	.225
560	.000000127	.225
760	.000000138	.225

TABLE VI Glass-Epoxy Thermophysical Properties

Density: 0.0707 lb/in^3

Temperature °R	Conductivity BTU/In-SEC-°R	Specific Heat BTU/lb - °R	Emittance
360	.0000043	.225	.876
560	.0000050	.225	.878
760	.0000054	.225	.892

TABLE VII Final-Attachment-Line-Gasket Thermophysical Properties

Density: 0.035 lb/in^3

Temperature °R	Conductivity BTU/IN-SEC°R	Specific Heat BTU/lb °R	Emittance
530	.00000241	.33	.910
610	.00000241	.33	.895

TABLE VIII Values of $\dot{q}/\dot{q}_s$ for Three-Dimensional Windward Corner Analyses, From Reference 7

TIME* SEC	$\dot{q}/\dot{q}_s$ Location A **	$\dot{q}/\dot{q}_s$ Location B	$\dot{q}/\dot{q}_s$ Locations C, D, and E
3.3	.88	.96	.17
4.3	.82	.88	.09
5.9	.735	.81	.08
8.2	.70	.84	.065
16.5	.52	.88	.060
Subsonic	1.0	1.0	1.0

* Time from 325000 FT

** See Figure 7 for Locations

TABLE IX Summary of Surface Recession Predictions and Virgin Ablator Thicknesses Remaining, Three Dimensional Windward Corner Analyses

			Nominal Heating		Factored Heating	
Location*	Ablative Material	Original Thickness Inches	Surface Recession Inches	Virgin Mat'l Remaining Inches	Surface Recession Inches	Virgin Mat'l Remaining Inches
A	PAET 28	.300	0.002	.173	0.022	.152
B	PAET 28	.420	0.024	.272	0.079	.239
C	PAET 28	.420	0.000	.385	0.000	.370
D	SLA 220	.25	0.000	.193	0.000	.167
E	SLA 220	.25	0.000	.193	0.000	.167

*See Figure 7 for locations

TABLE X. PLASMA ARC SPECIMEN THERMOCOUPLE LOCATIONS

Specimen No.	Distance From Ablator Surface - Inches		
	T/C#1	T/C#2*	T/C#3**
	THREE-INCH DIAMETER SPECIMENS		
2-1-1	.16	.26	.76
2-1-2	.15	.25	.72
2-1-3	.17	.26	.72
2-1-4	.16	.26	.73
2-1-5	.15	.26	.74
2-1-6	.15	.25	.73
2-1-7	.16	.25	.72
2-1-8	.15	.26	.75
2-1-9	.14	.25	.75
2-1-10	.11	.23	.74
	ELEVEN-INCH DIAMETER SPECIMENS		
2-2-1	.16	.25	.73
2-2-2	.12	.25	.78
2-2-3	.11	.24	.74

* At the SLA-220/Honeycomb-Sandwich Bond Line

** On the Exterior of the Honeycomb Sandwich Backface

VIII FIGURES

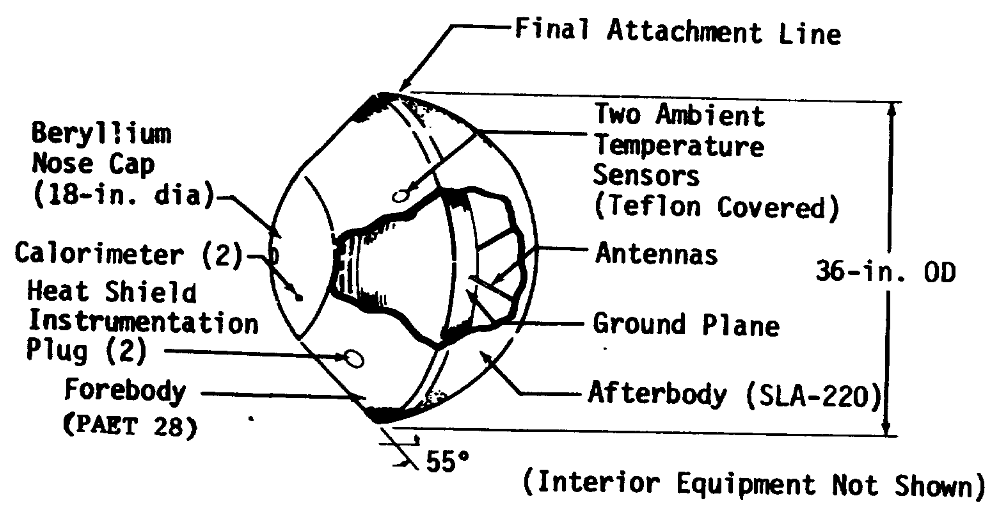

FIGURE 1 PAET Probe

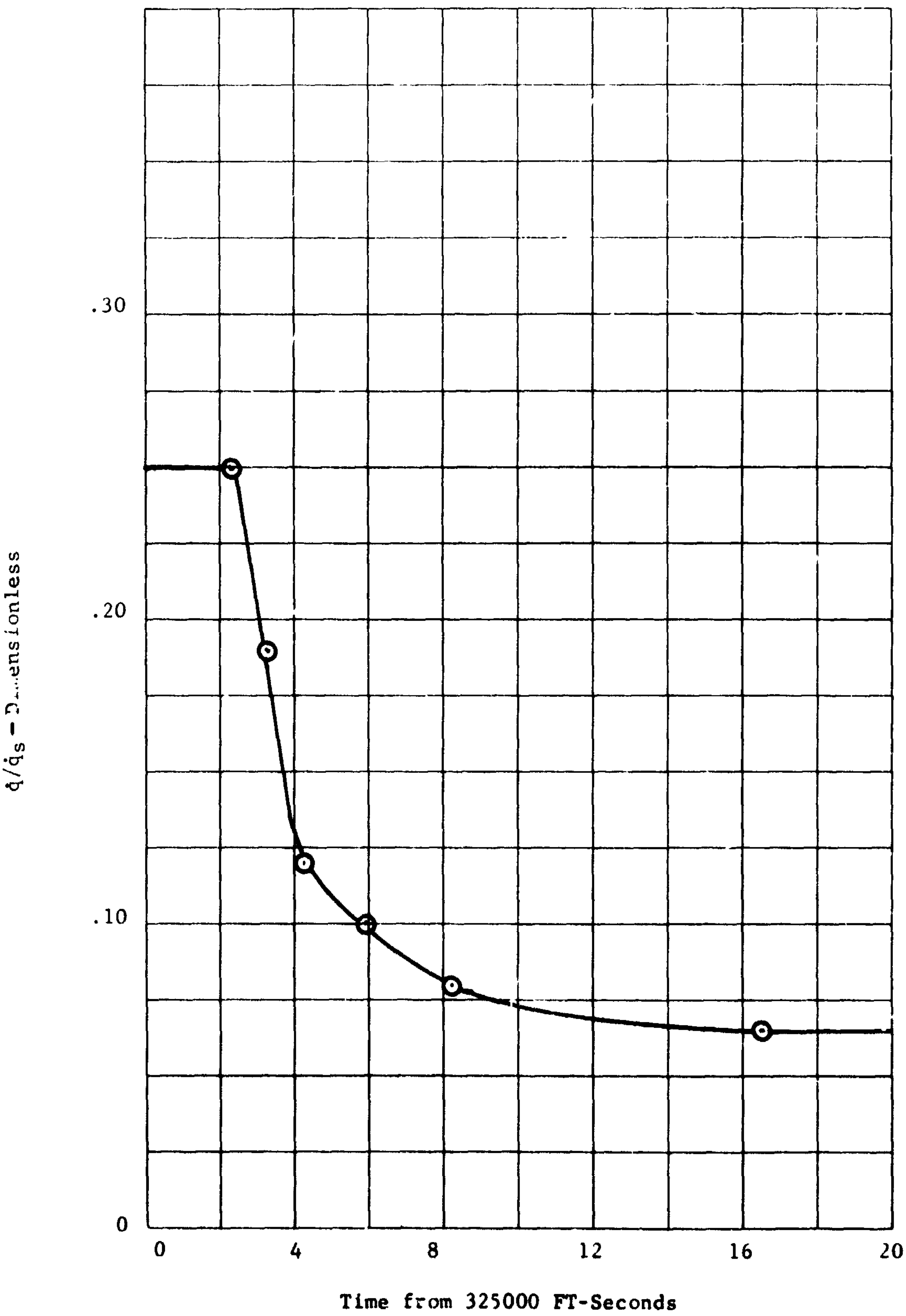

Figure 2. Variable $\dot{q}/\dot{q}_s$ for One-Dimensional Thermal Analysis

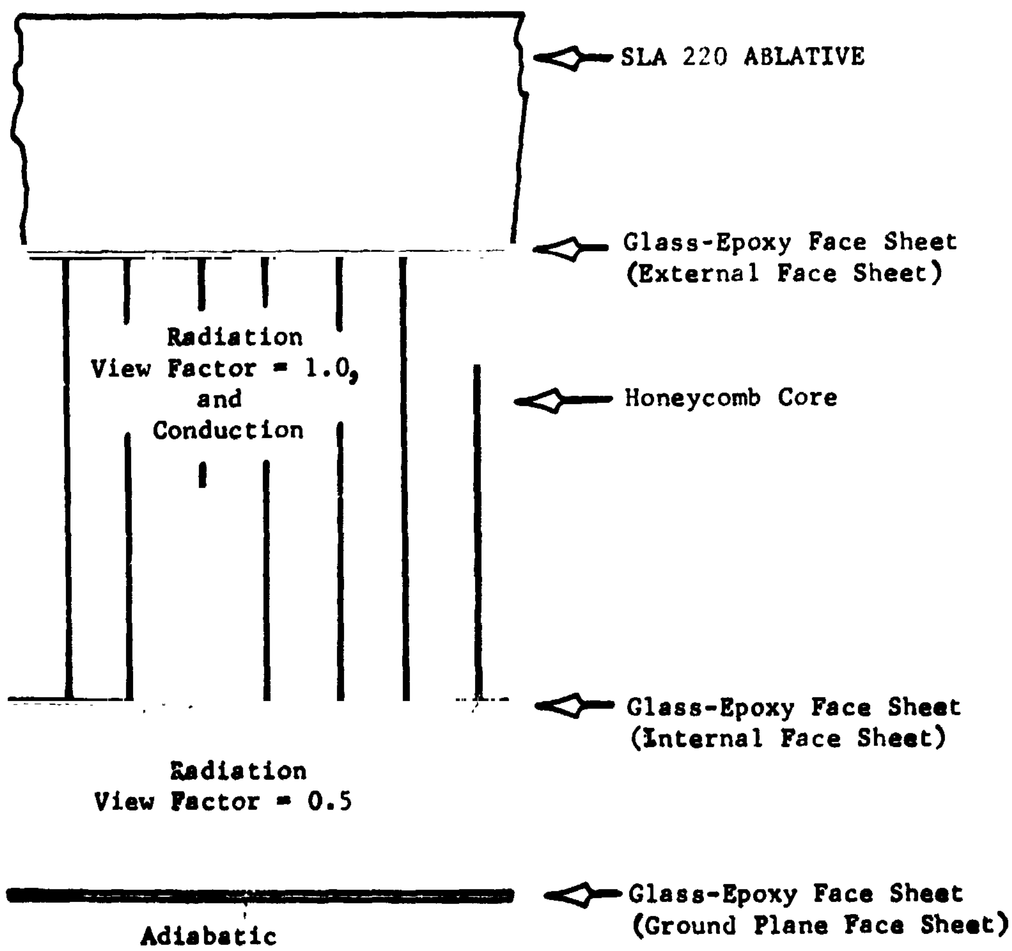

Figure 3 - Model for One-Dimensional PAET Afterbody Thermal Analysis

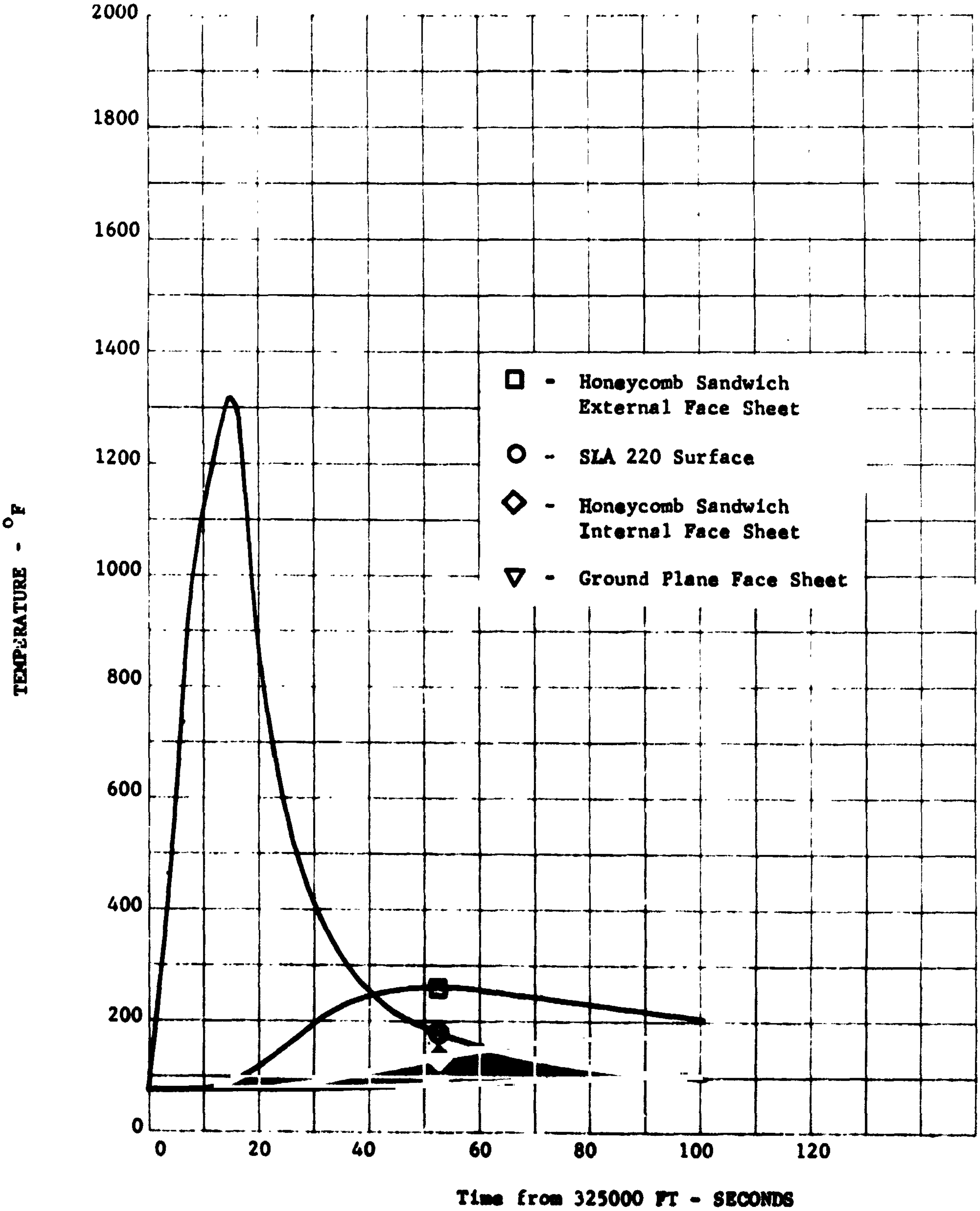

FIGURE 4 - PAET Afterbody Thermal Response, $\dot{q}/\dot{q}_s$ = 0.05, One-Dimensional Analysis

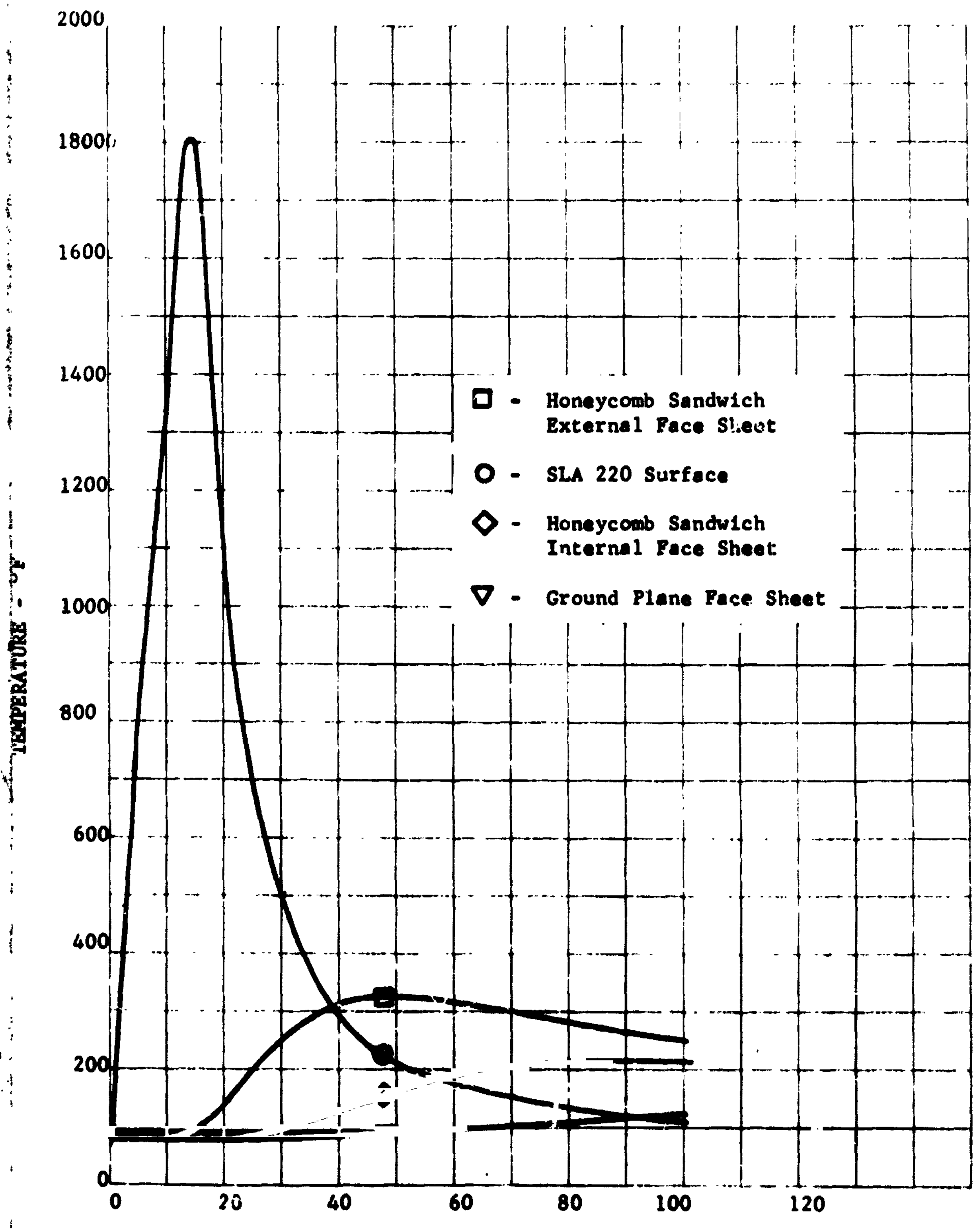

FIGURE 5 - PAET Afterbody Thermal Response, $\dot{q}/\dot{q}_s = 0.10$, One-Dimensional Analysis

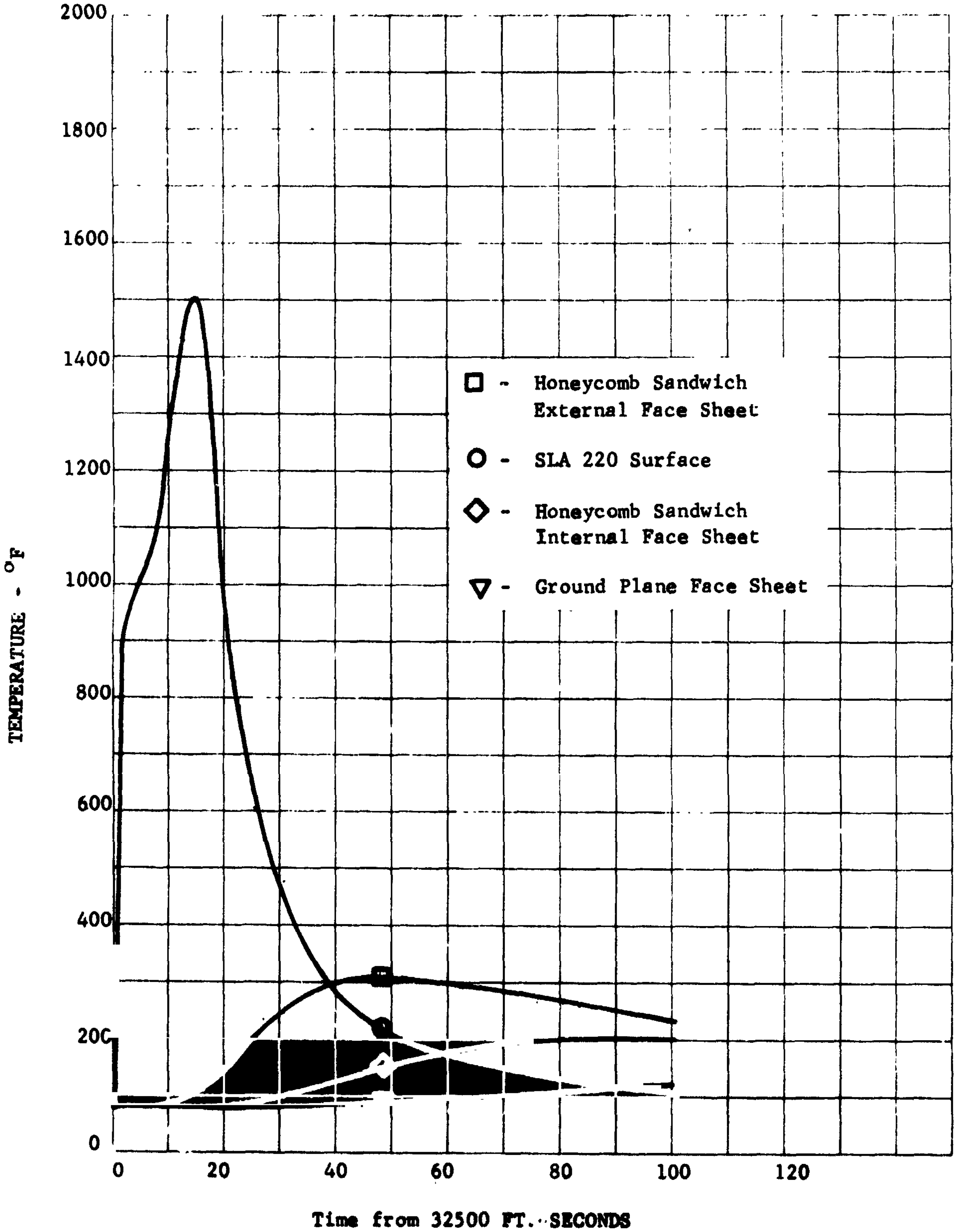

FIGURE 6. PAET Afterbody Thermal Response, Variable $\dot{q}/\dot{q}_b$, One-Dimensional Analysis

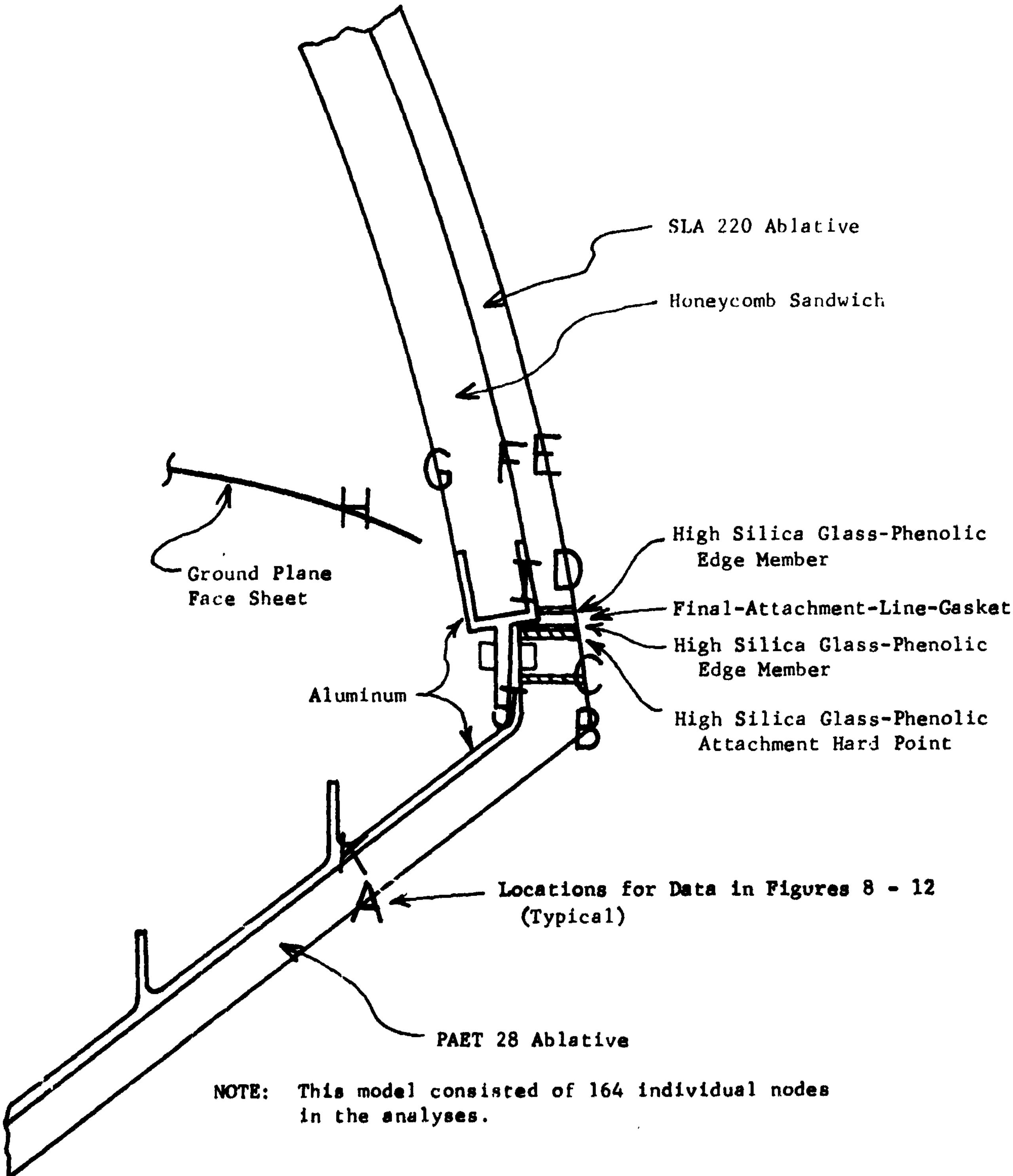

NOTE: This model consisted of 164 individual nodes in the analyses.

FIGURE 7. Model for Three-Dimensional Analysis of PAET Windward Corner

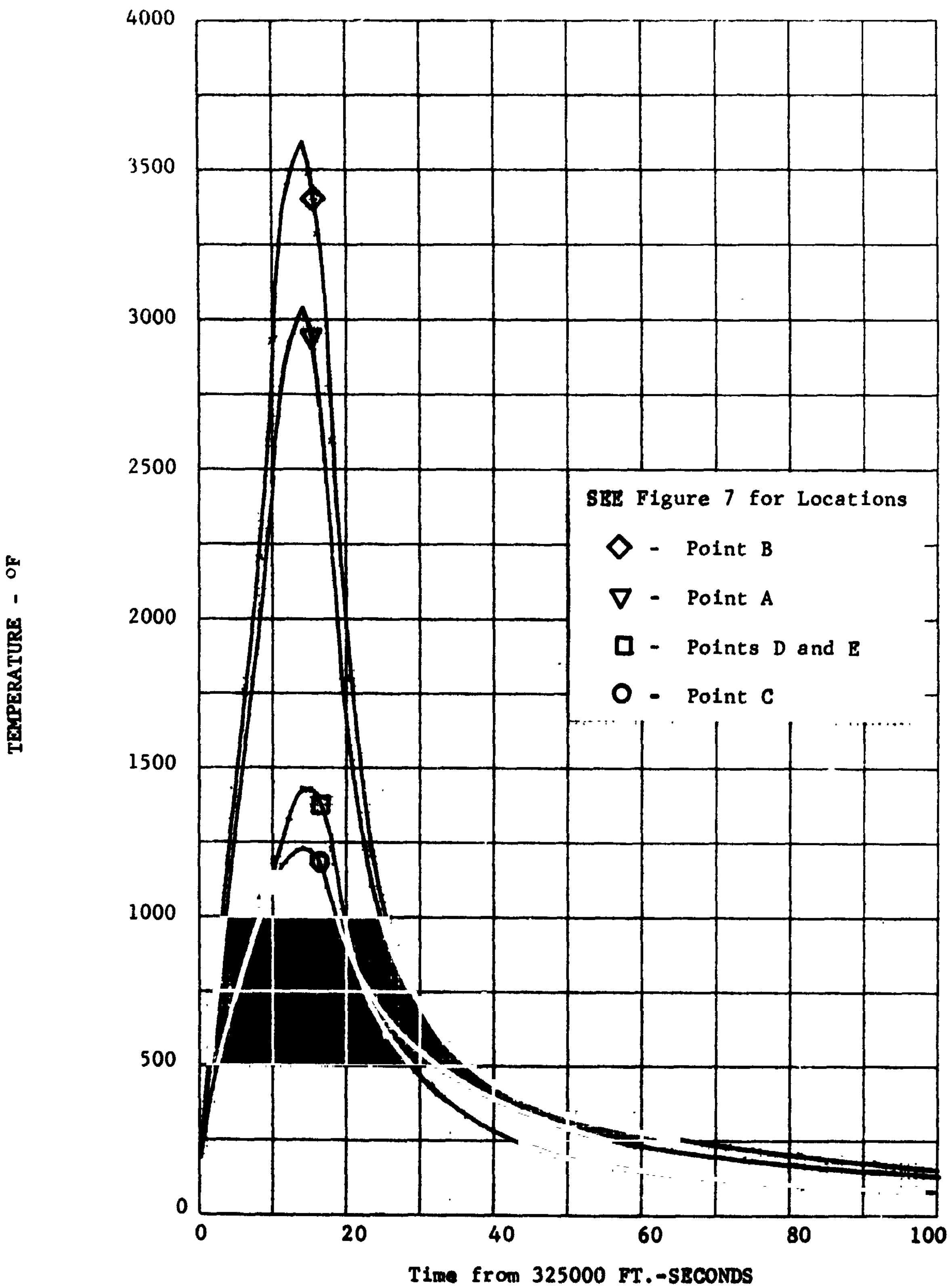

FIGURE 8. PAET Surface Temperature Response, Nominal Heating Distribution, Three-Dimensional Windward Corner Analysis

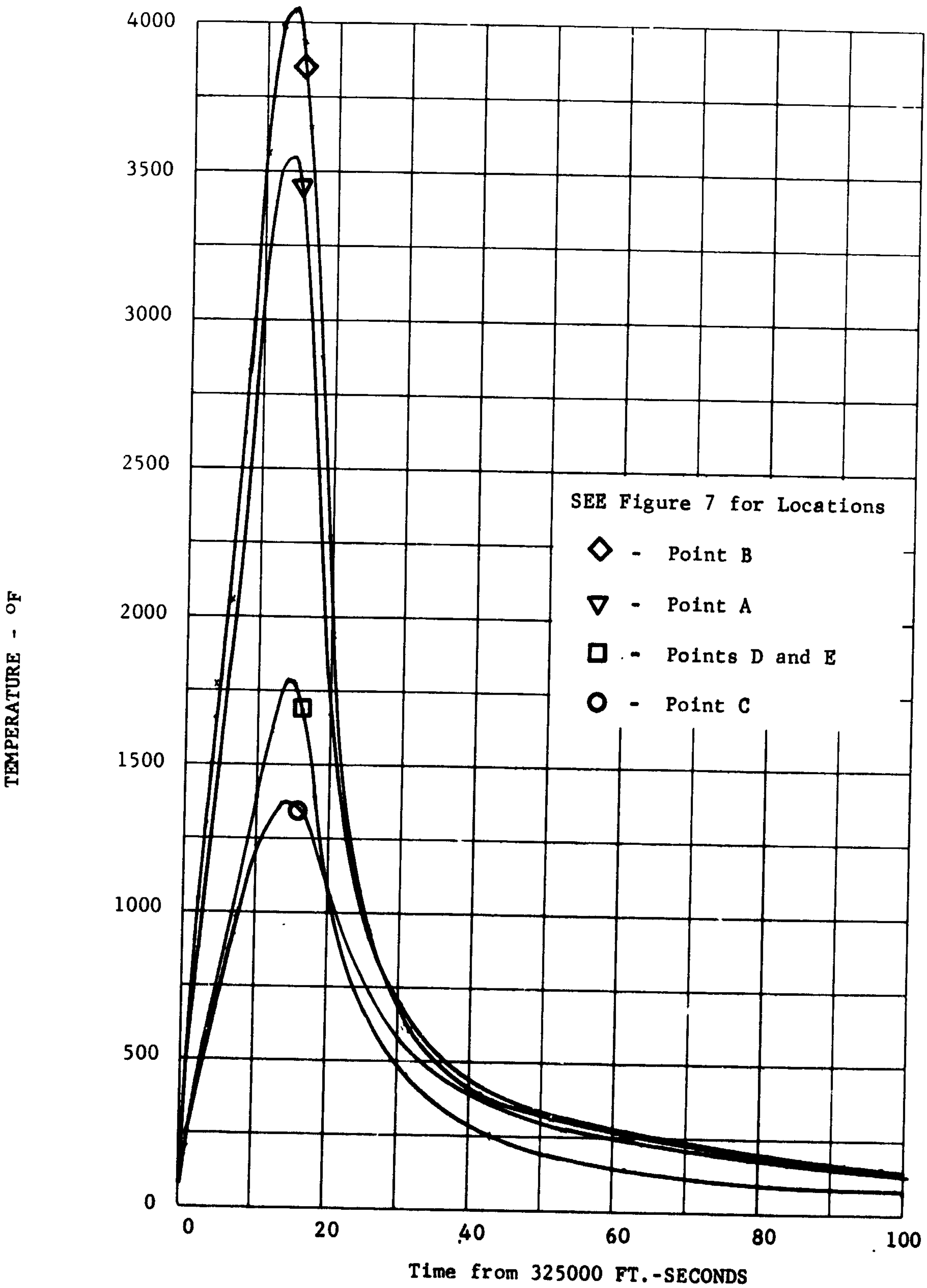

FIGURE 9. PAET Surface Temperature Response, 1.5 x Nominal Heating Distribution, Three-Dimensional Windward Corner Analysis

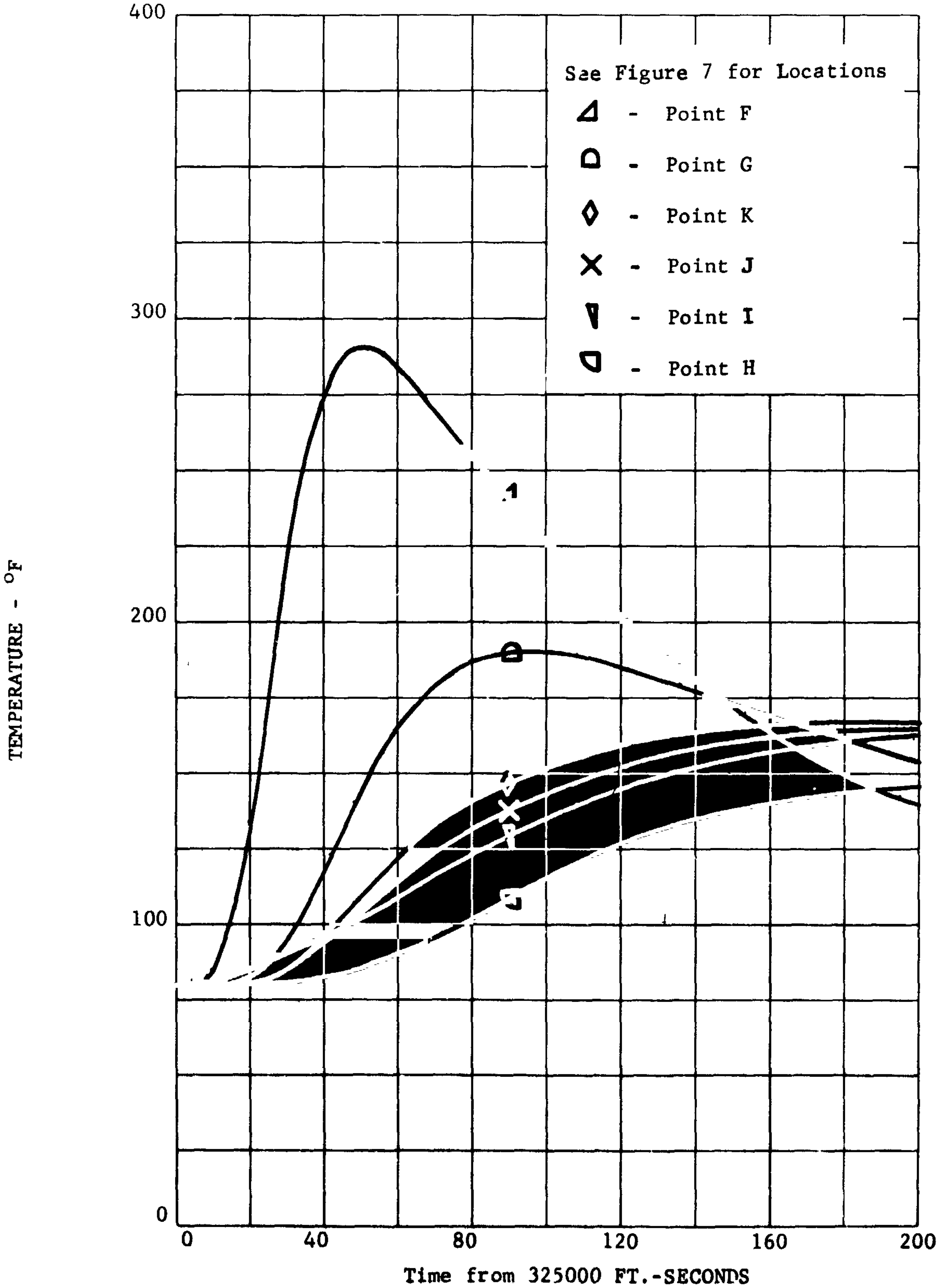

FIGURE 10. PAET Structure Temperature Response, Nominal Heating Distribution, Three-Dimensional Windward Corner Analysis

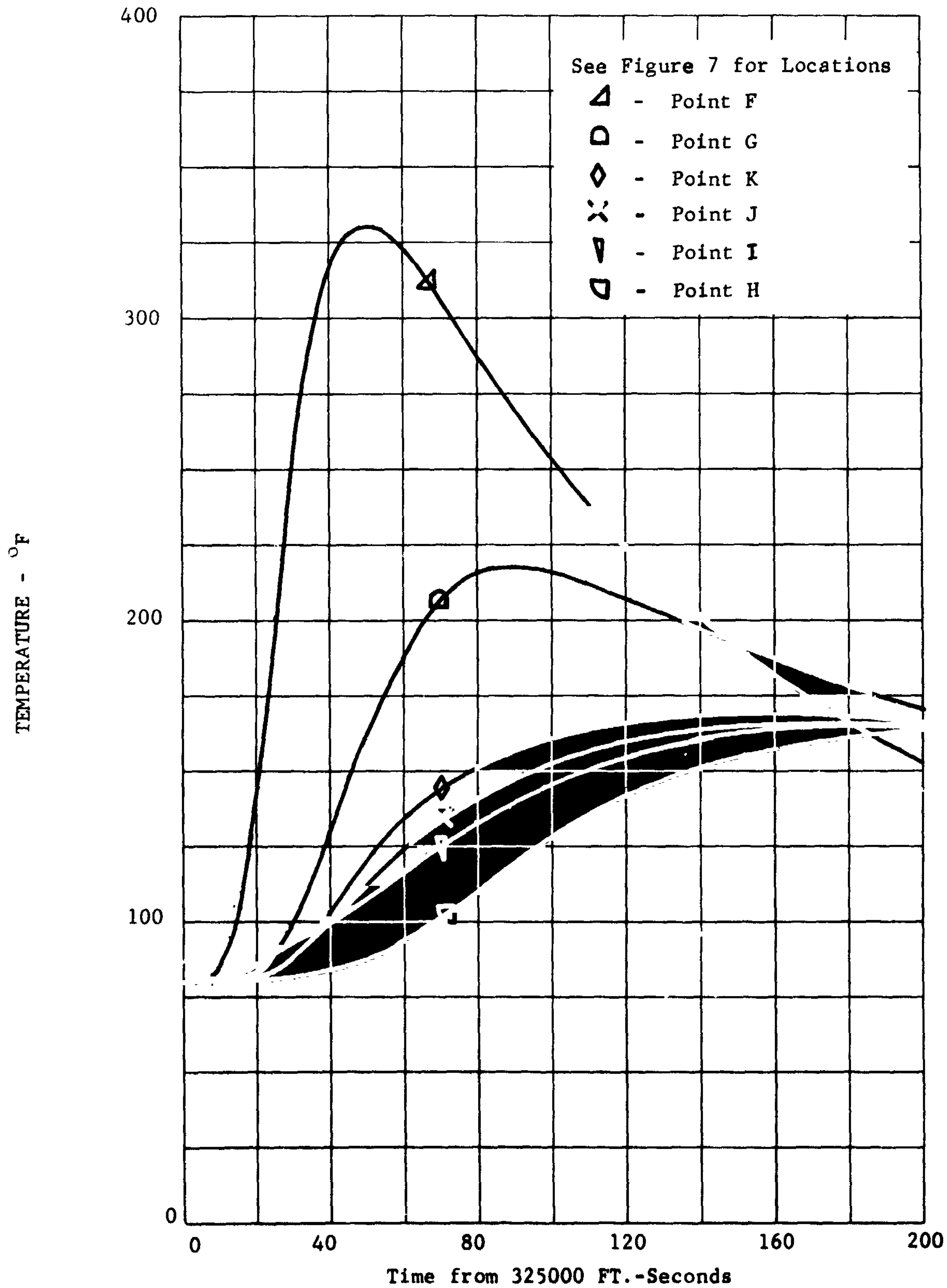

FIGURE 11. PAET Structure Temperature Response, 1.5 x Nominal Heating Distribution, Three-Dimensional Windward Corner Analysis

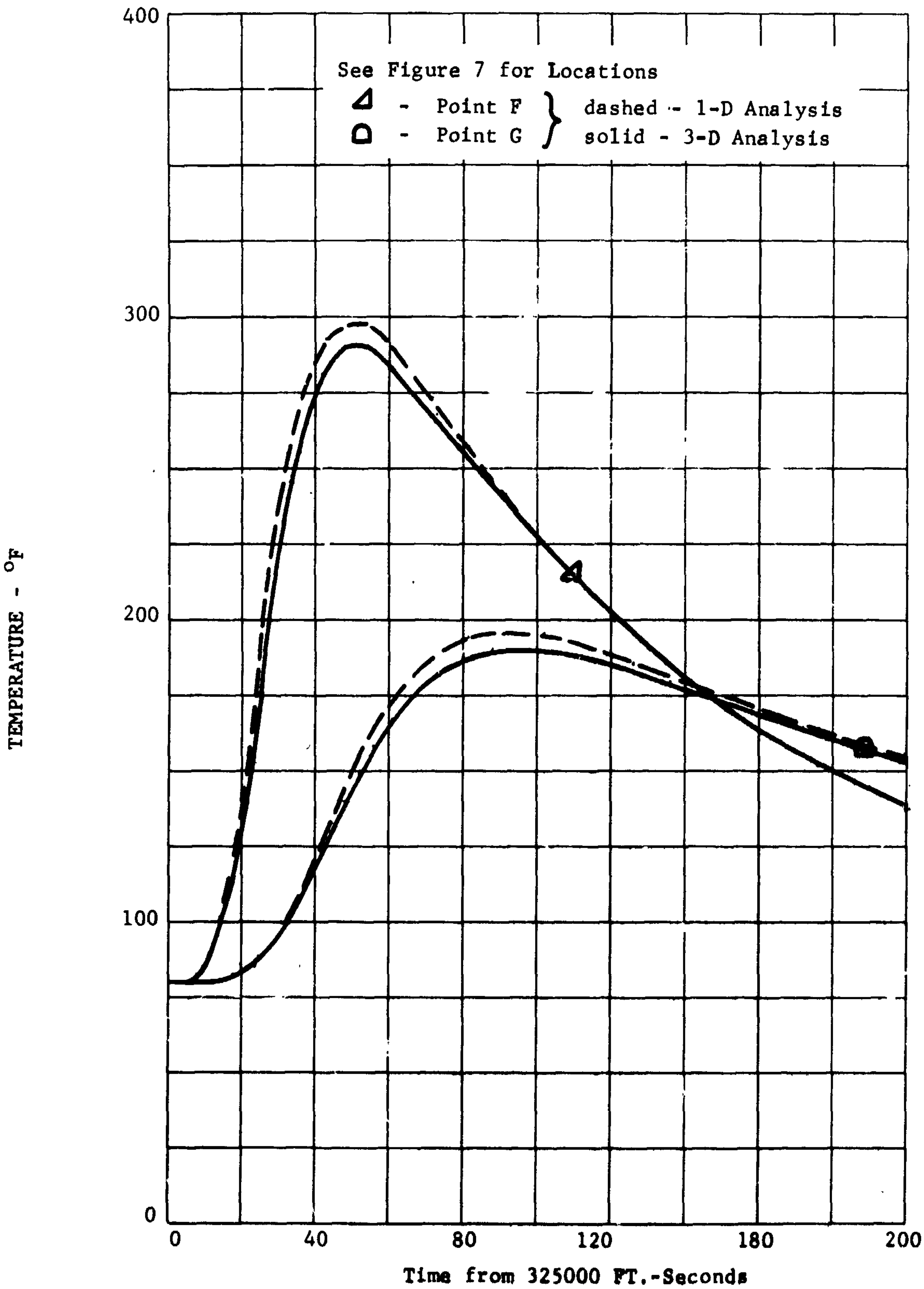

FIGURE 12. Comparison of One-Dimensional and Three-Dimensional PAET Afterbody Thermal Response, Nominal Heating Distribution

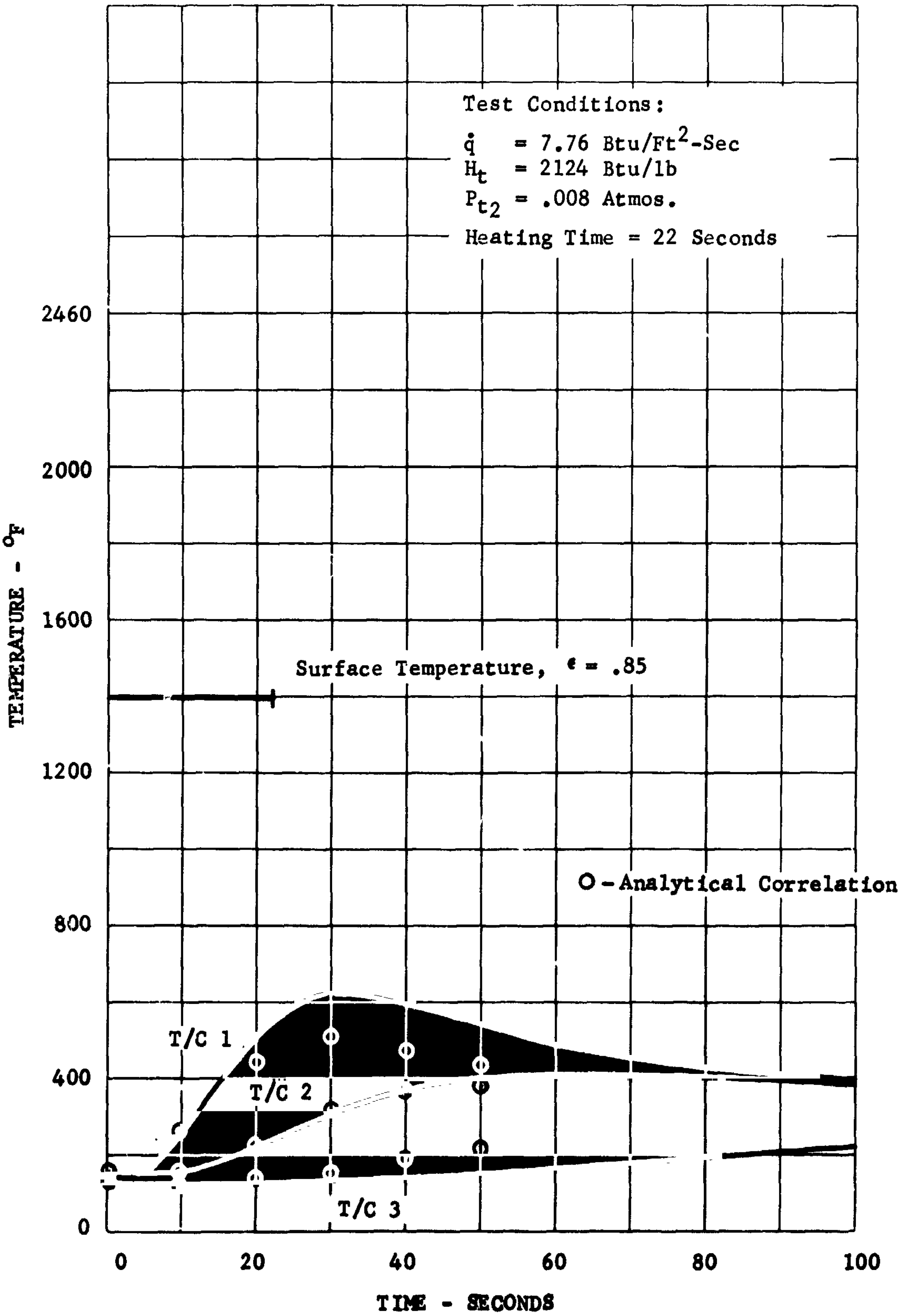

FIGURE 13. Plasma Arc Specimen 2-2-1 Thermal Response

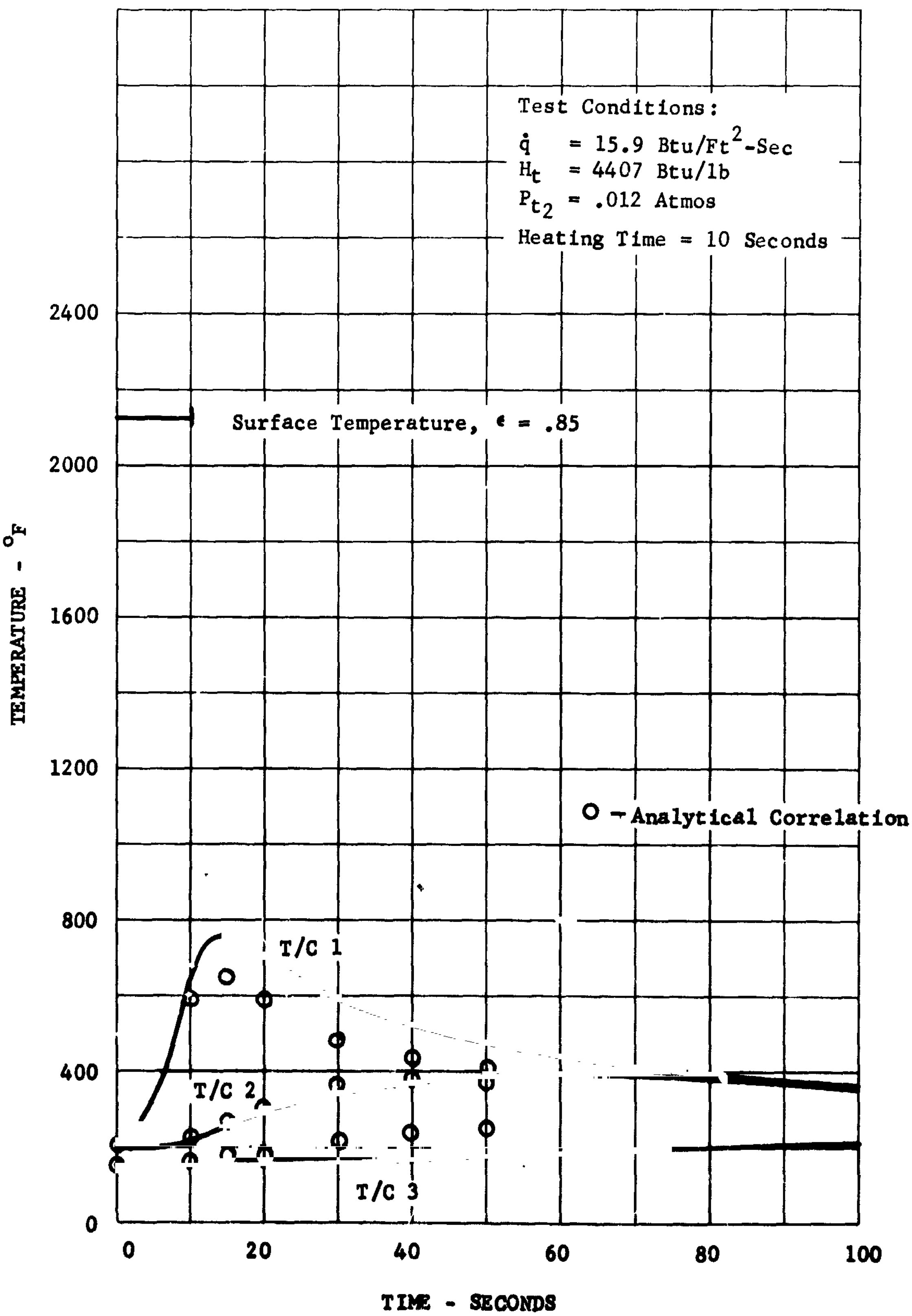

FIGURE 14. Plasma Arc Specimen 2-2-2 Thermal Response

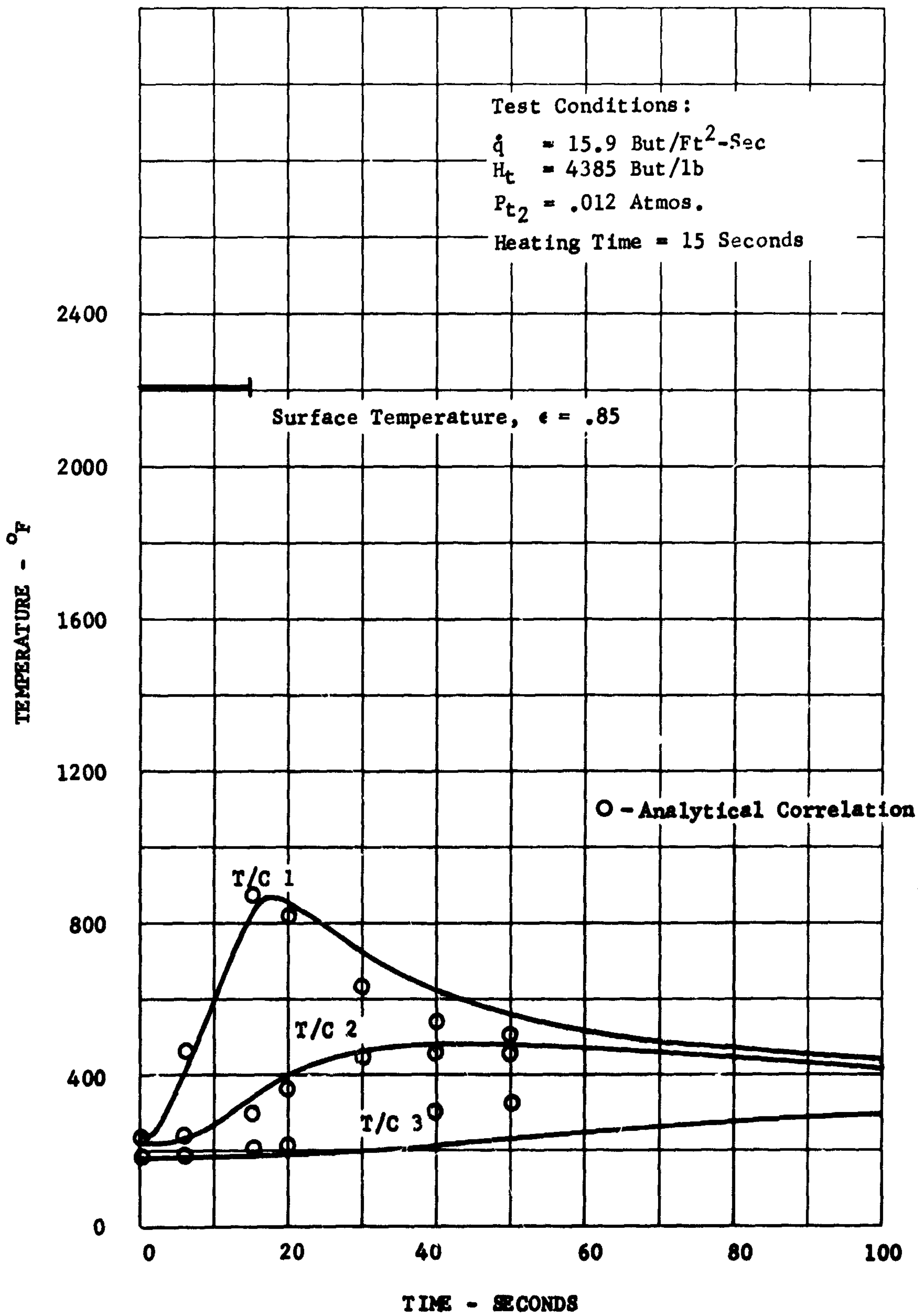

FIGURE 15. Plasma Arc Specimen 2-2-3 Thermal Response

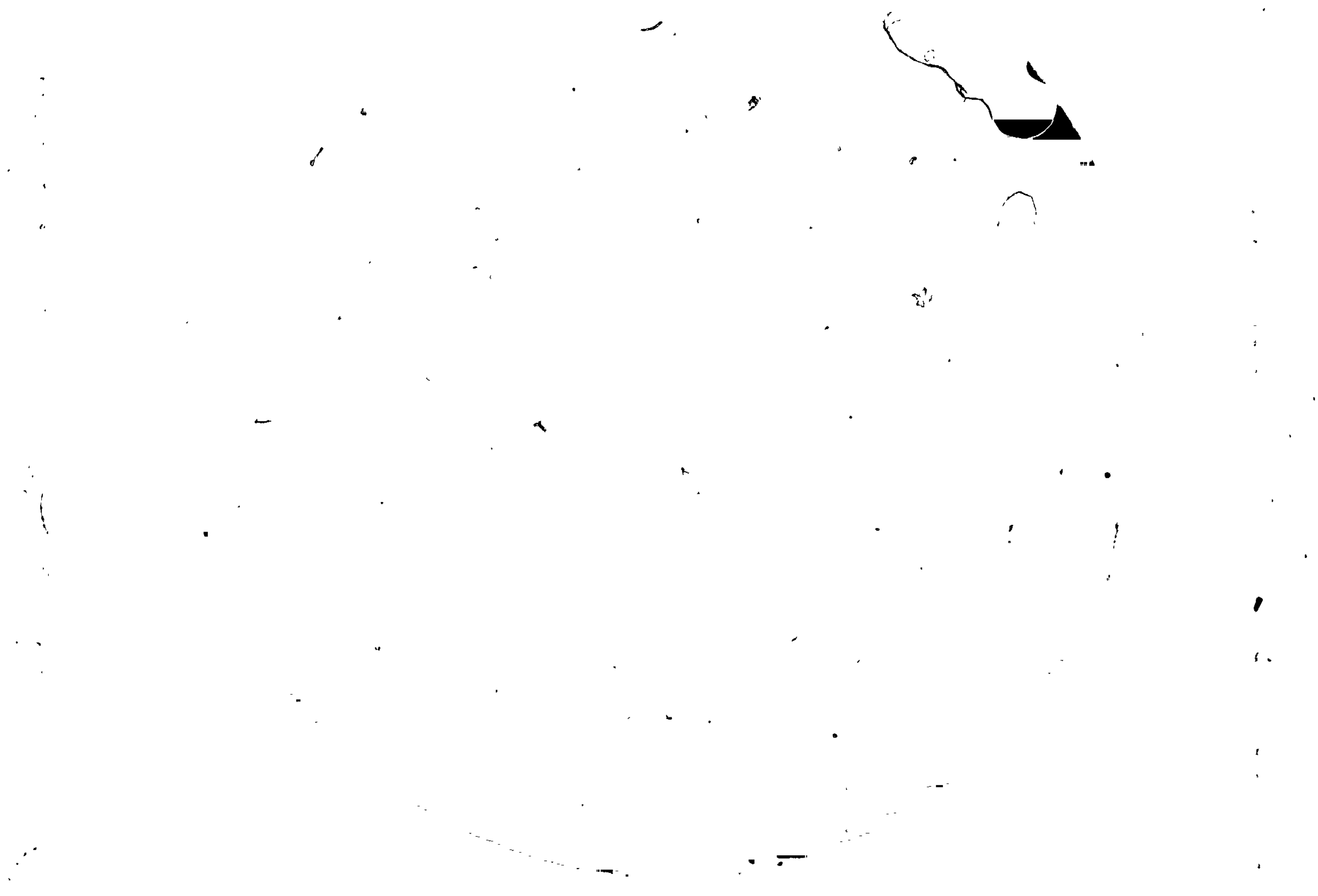

FIGURE 16. Plasma Arc Specimen 2-2-1 After Test

FIGURE 17. Plasma Arc Specimen 2-2-2 After Test

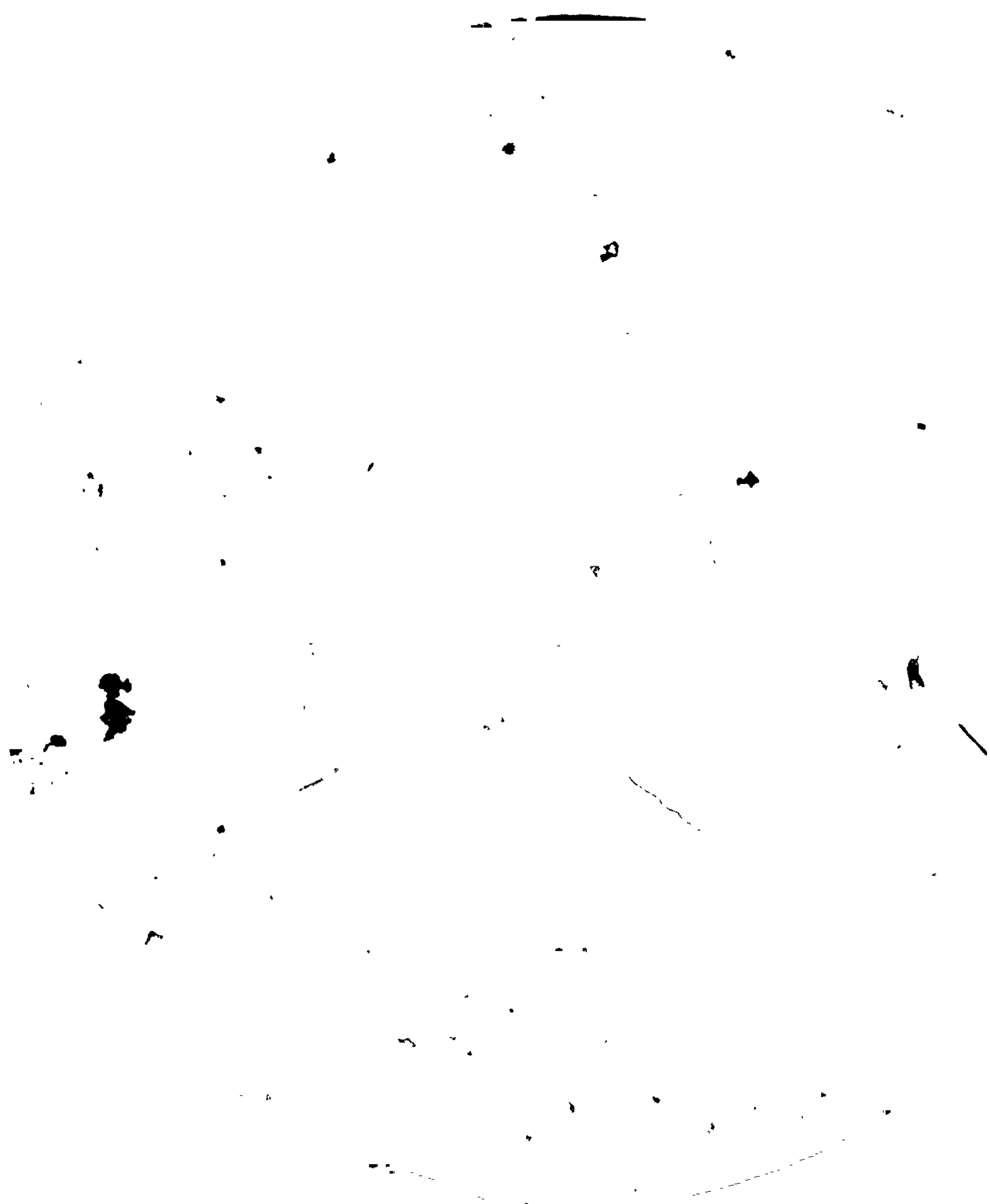

FIGURE 18. Plasma Arc Specimen 2-2-3 After Test

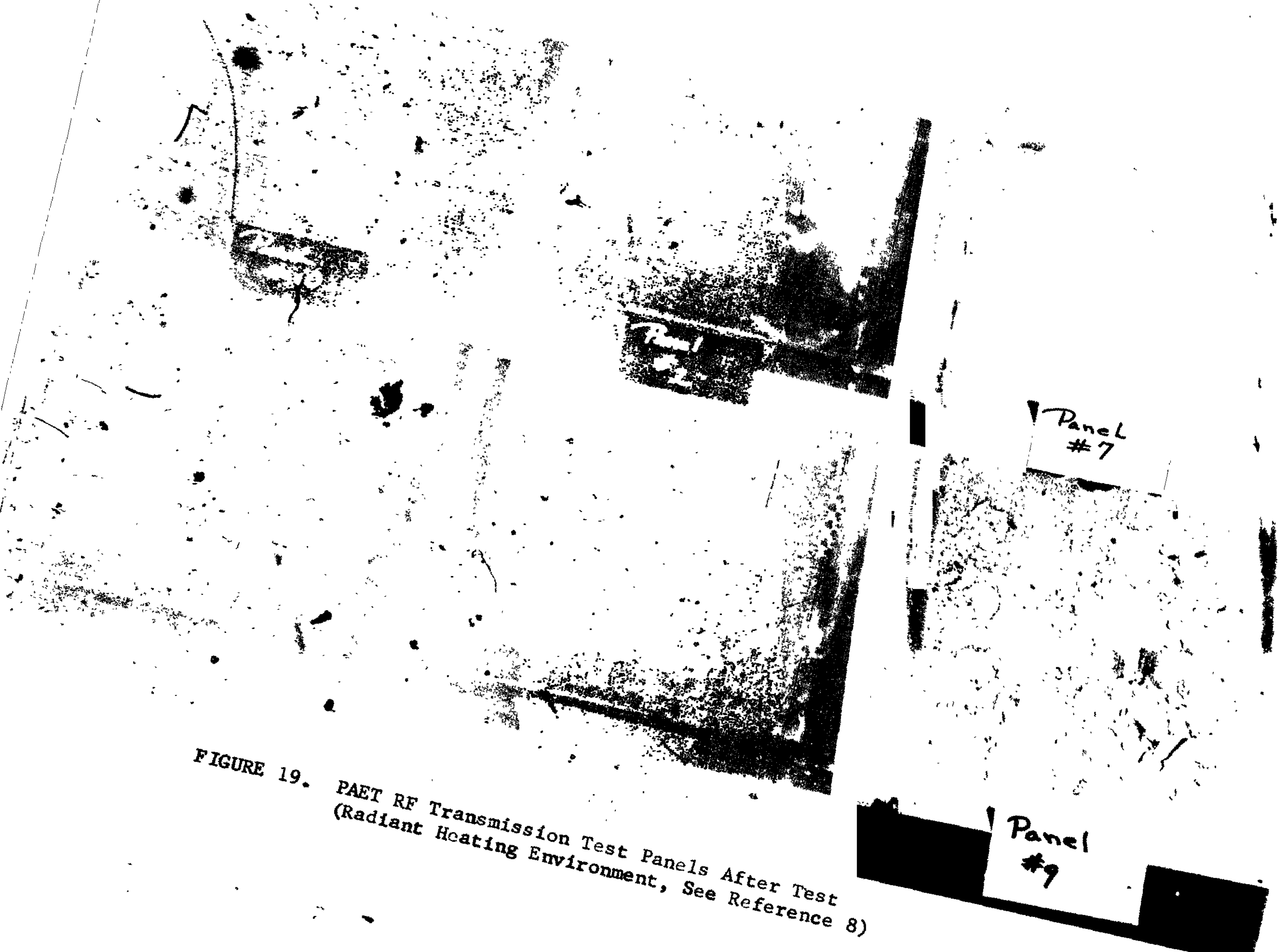

FIGURE 19. PAET RF Transmission Test Panels After Test (Radiant Heating Environment, See Reference 8)

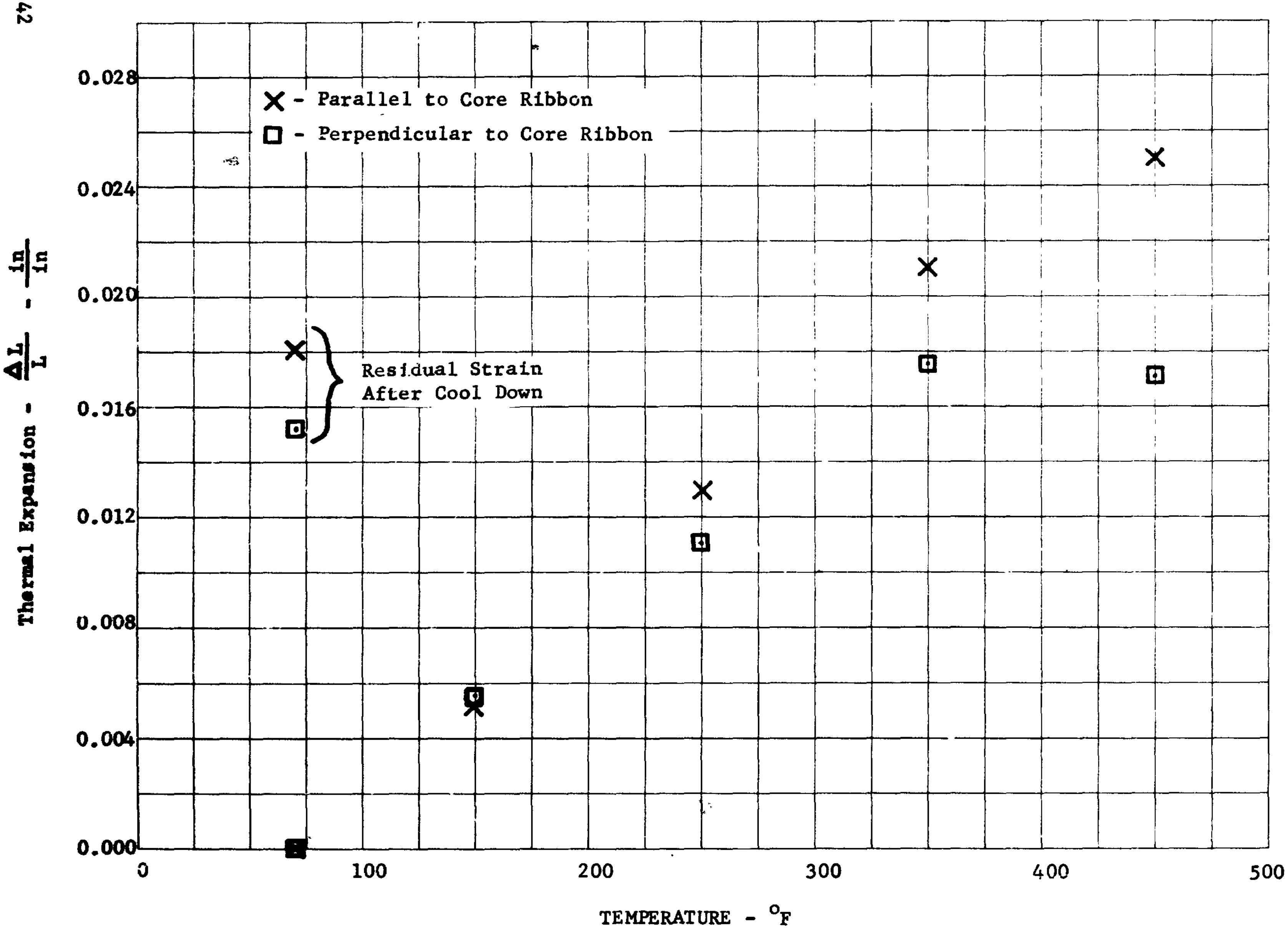

FIGURE 20. PAET-Honeycomb-Sandwich Thermal Expansion Data

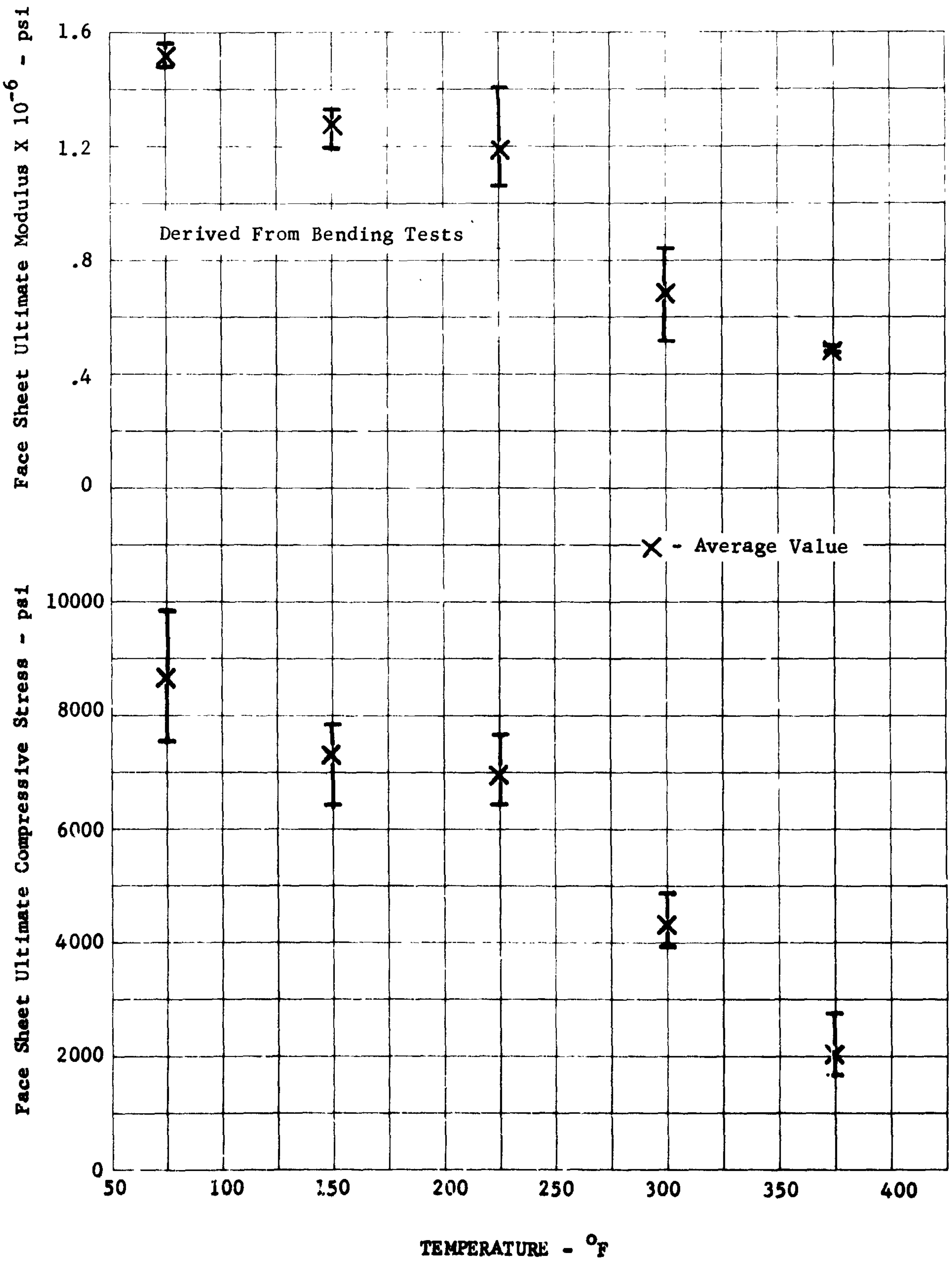

FIGURE 21. **PAET-Honeycomb-Sandwich Flexure Strength and Modulus Parallel to Core Ribbon**

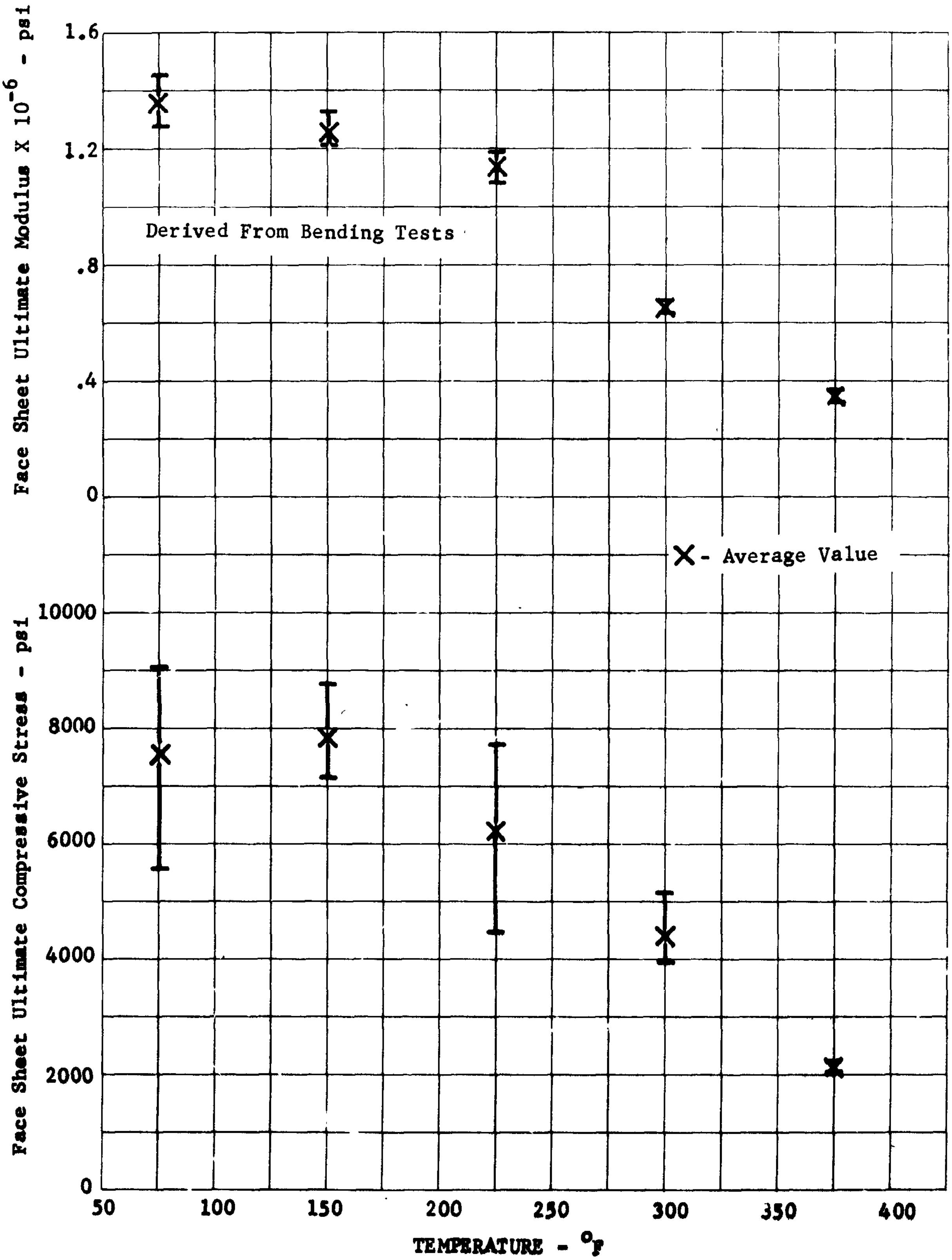

FIGURE 22. PAET-Honeycomb-Sa
Perpendicula

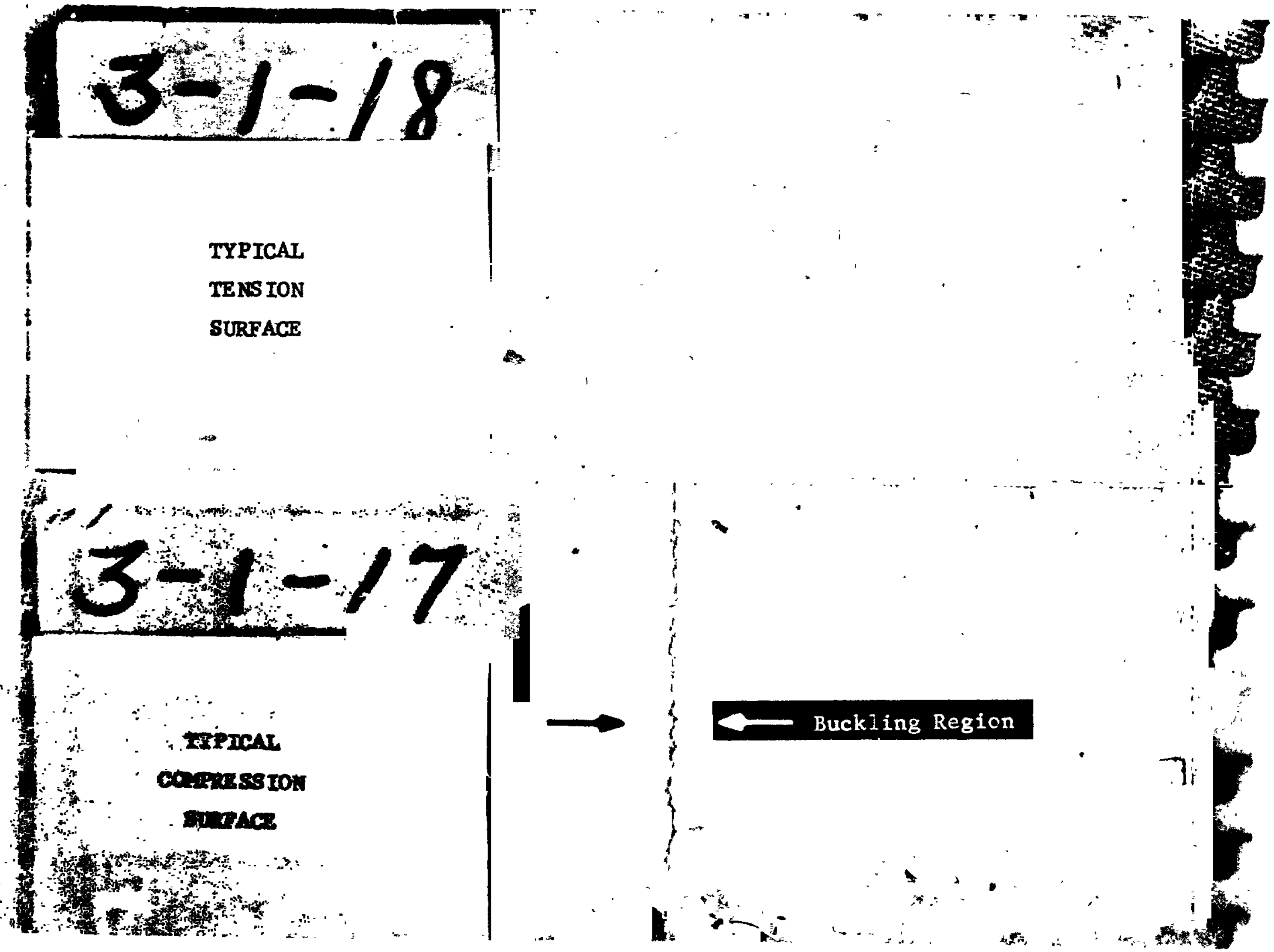

FIGURE 23. Typical PAET-Honeycomb-Sandwich Flexure Specimen After Test

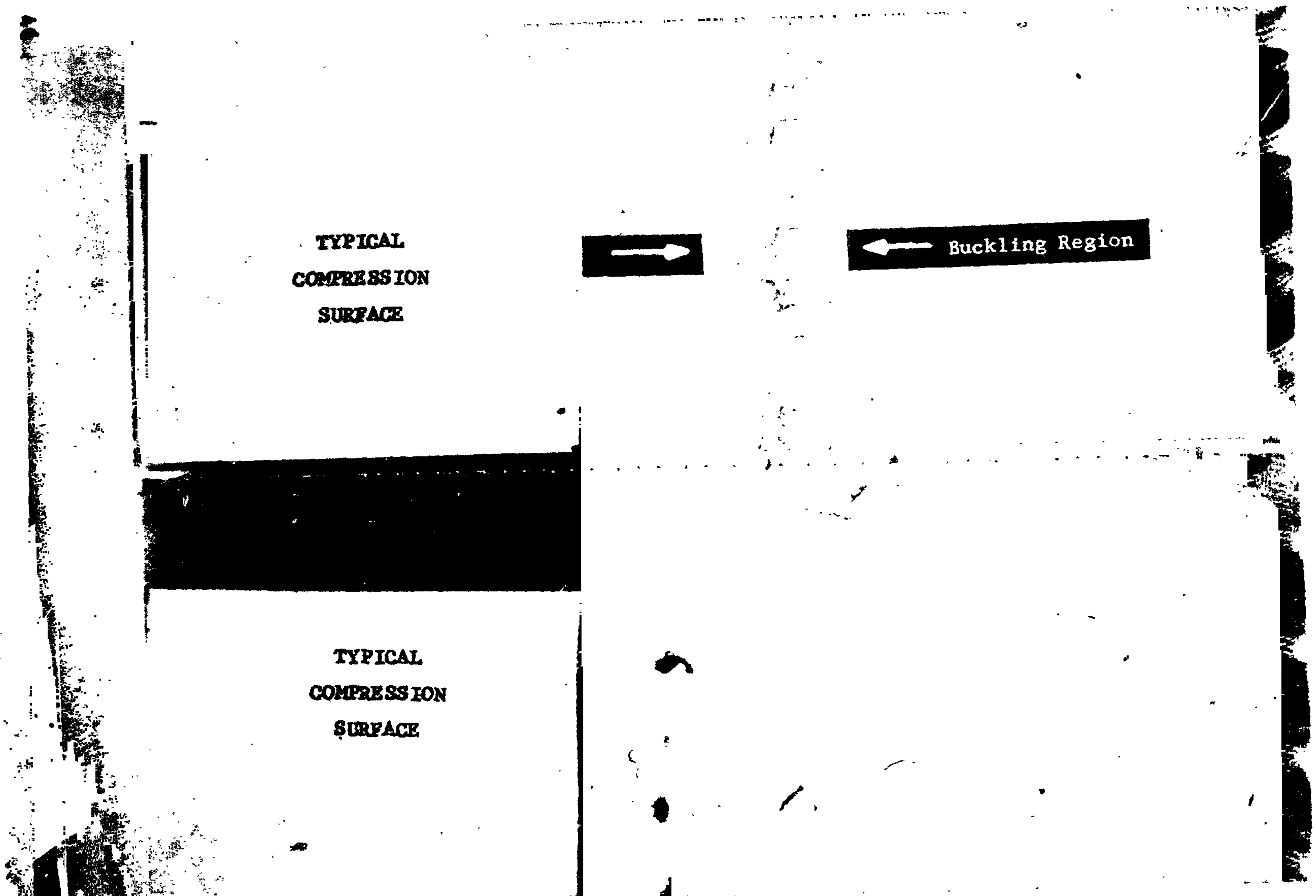

FIGURE 24. Typical PAET-Honeycomb-Sandwich Flexure Specimen After Test

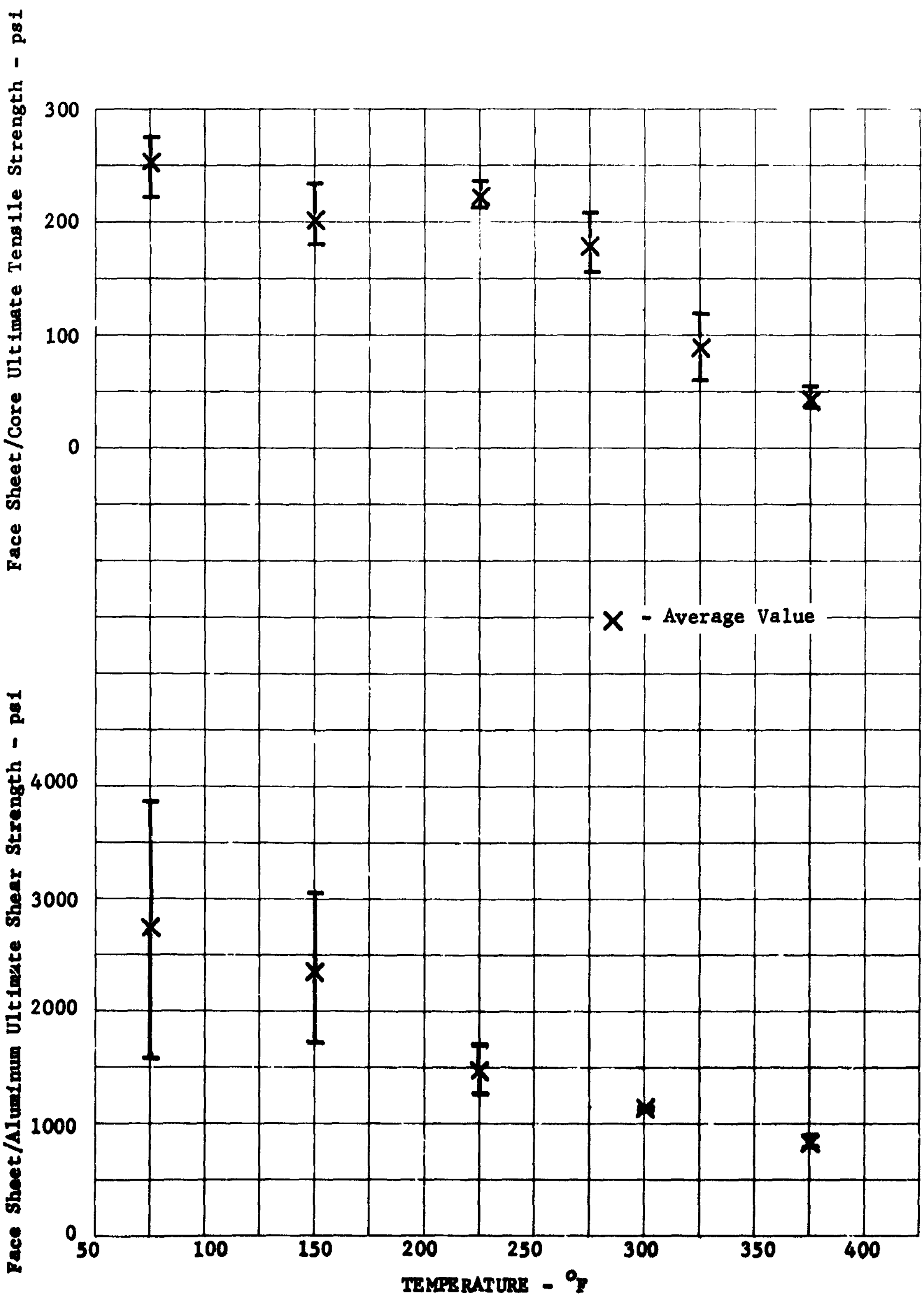

FIGURE 25. PAET-Honeycomb-Sandwich Face-Sheet-To-Core Tensile and Face-Sheet-To-Aluminum Shear Strength

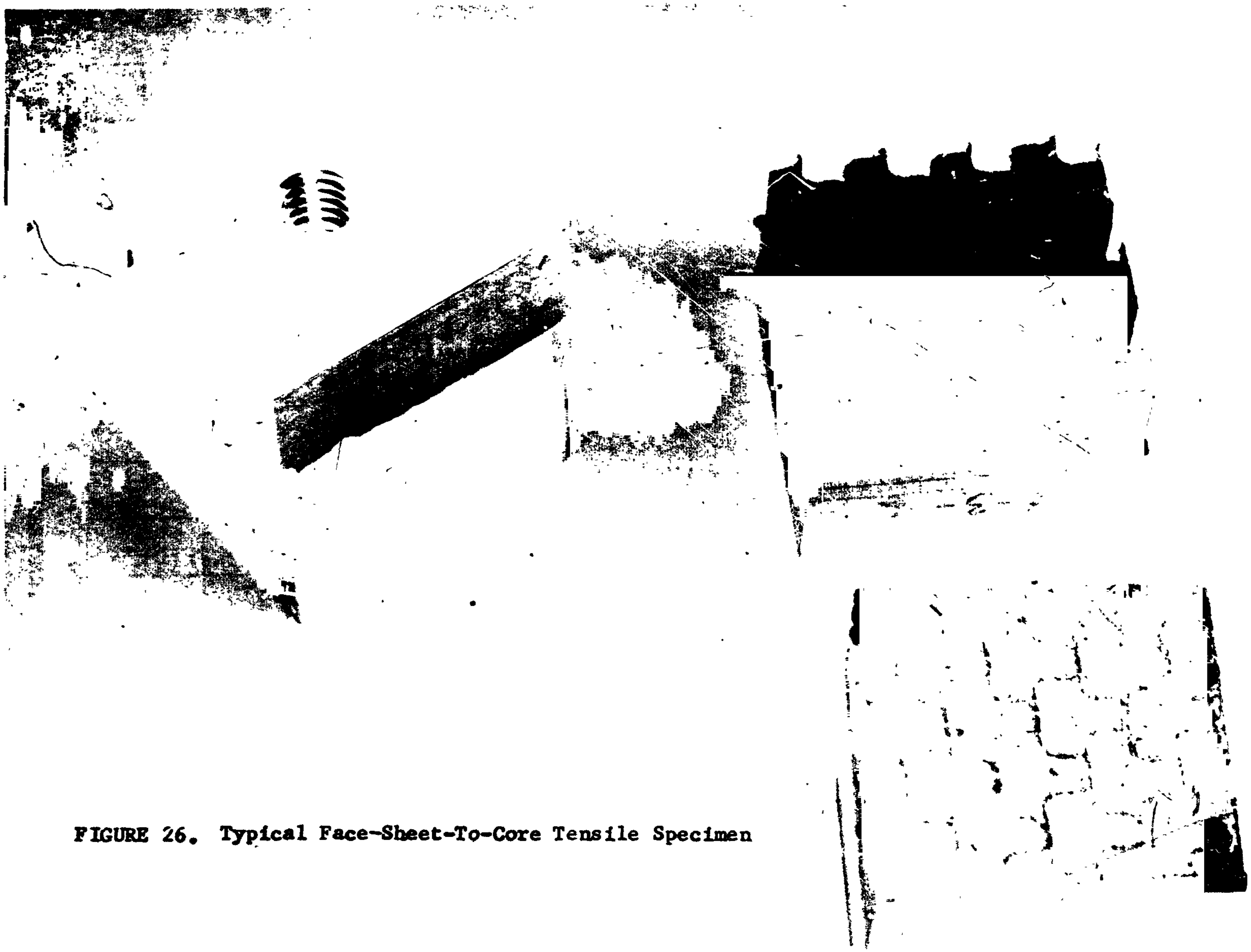

FIGURE 26. Typical Face-Sheet-To-Core Tensile Specimen

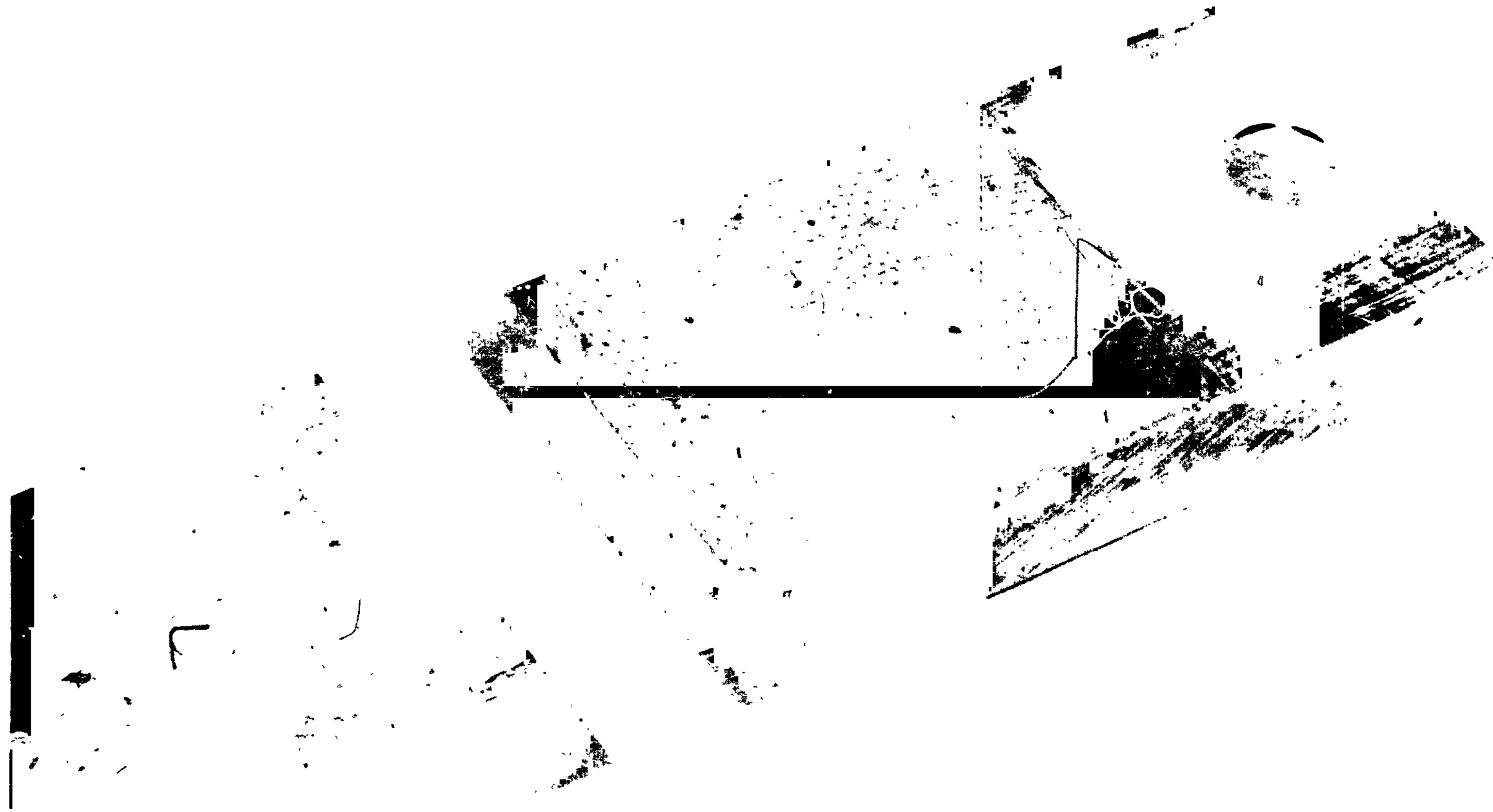

FIGURE 27. Typical Face-Sheet-To-Aluminum Lap Shear Specimen

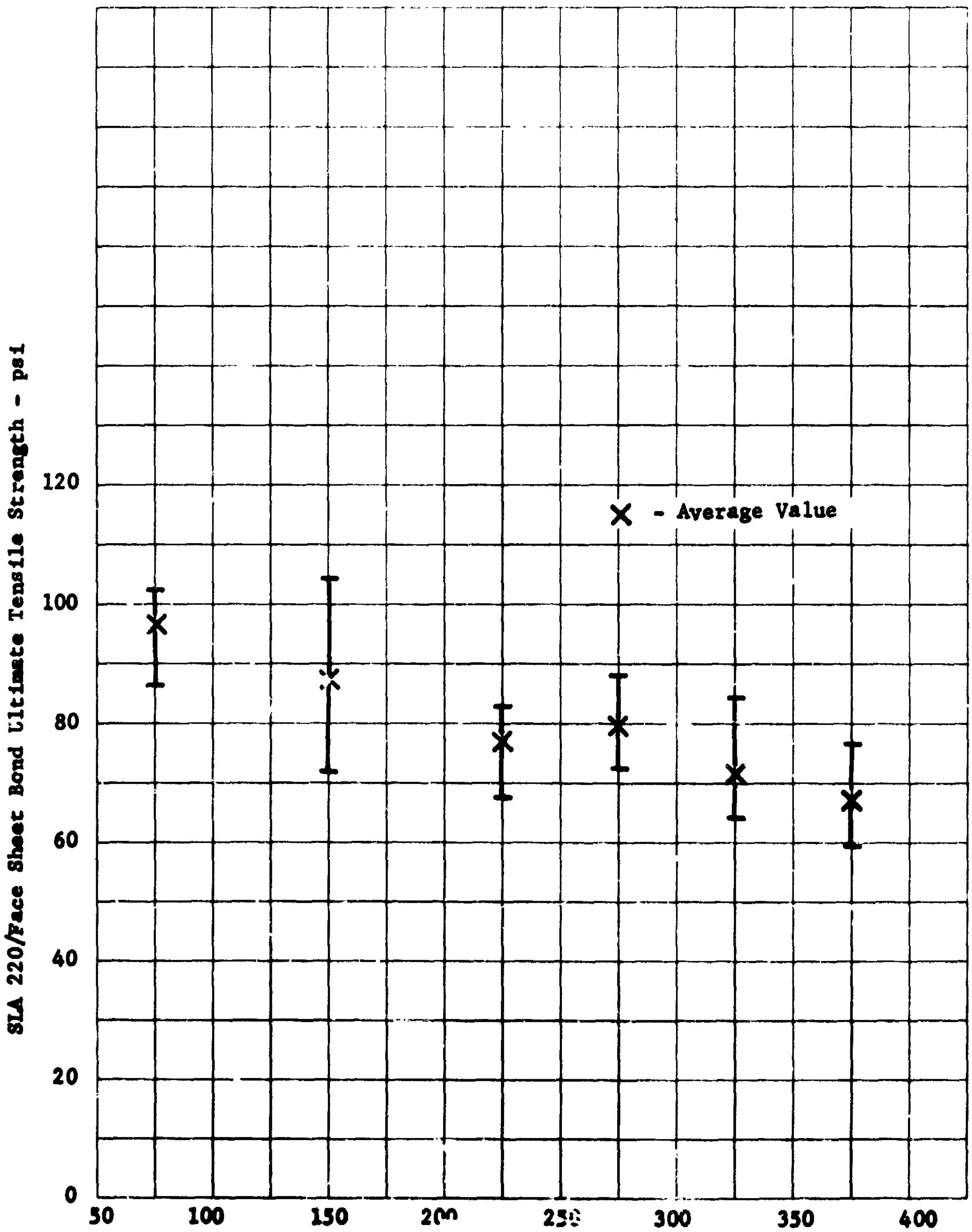

FIGURE 28. SLA 220/PAET-Honeycomb-Sandwich-Face-Sheet Bond Ultimate Tensile Strength

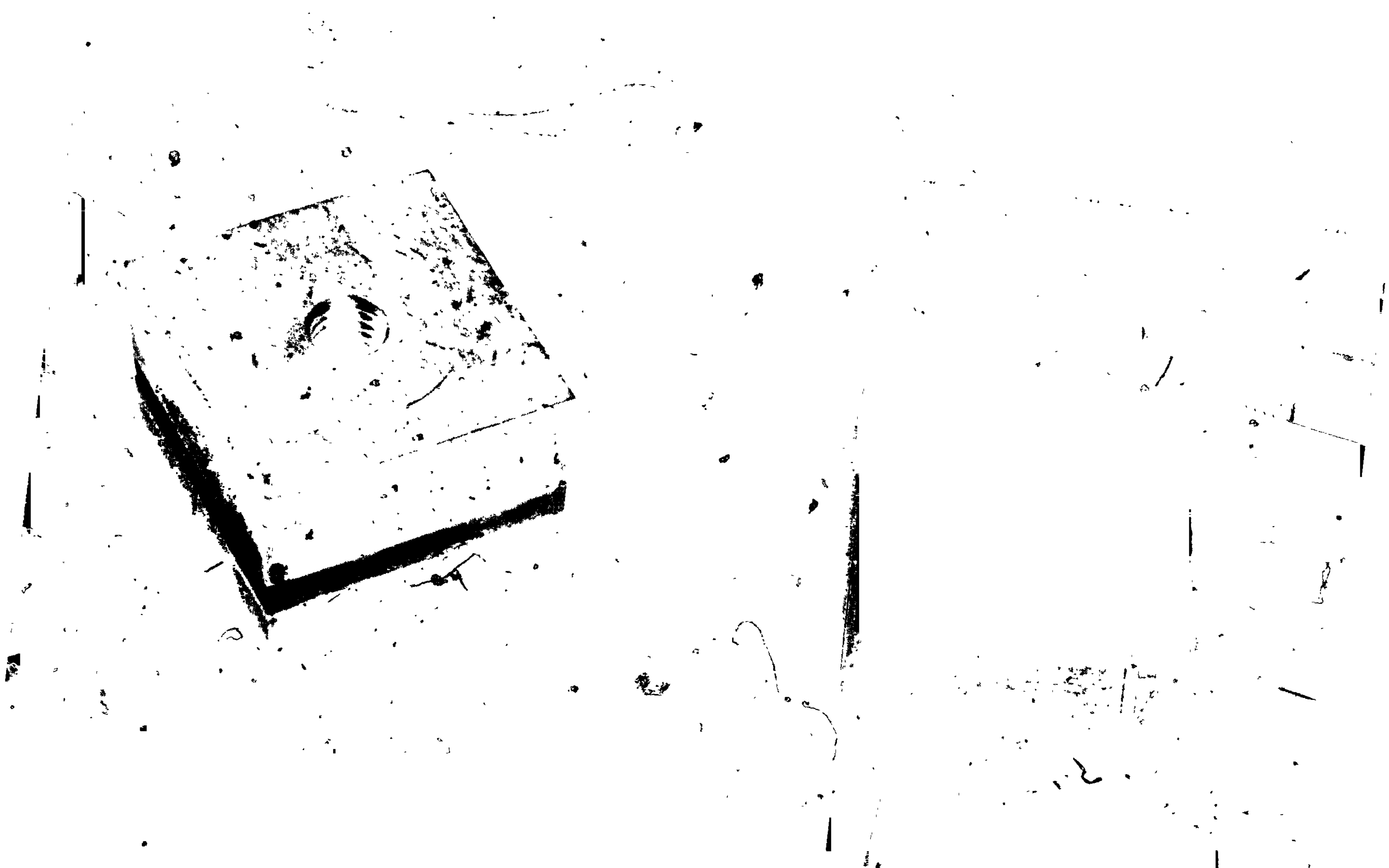

FIGURE 29. Typical SLA 220-To-Face-Sheet Tensile Specimen

END.
5/11/71